TOWARDS REALISTIC HAPTIC RENDERING OF SURFACE TEXTURES

A Thesis

Submitted to the Faculty

of

Purdue University

by

Seungmoon Choi

In Partial Fulfillment of the

Requirements for the Degree

of

Doctor of Philosophy

December 2003

This dissertation is dedicated to my parents, Sooah and Soojung.

ACKNOWLEDGMENTS

I am sincerely thankful to my advisor, Prof. Hong Z. Tan. This dissertation would have not existed without her support and guidance. Hong has been the paragon of an academic advisor and a respectable human being. I also thank all other members in my doctoral committee, Prof. Kak, Prof. Maciejewski, and Prof. Pizlo, for their thoughtful comments on my thesis.

I greatly appreciate the help of the guys in the Haptic Interface Research Laboratory. They (Ali, Chanon, Jay, John, Laron, Sean, and Ryan; just in an alphabetical order) have been the best colleagues one can imagine. In addition, I am grateful to many Korean friends here at Purdue who have also traversed the hard life of studying abroad. I cordially wish them happiness.

I cannot dare to find words to express my gratitude to my parents. They have always been with me watching and supporting their son with never-ending trust. I would be never able to repay their love and sacrifice. Thank you to my little brother, Seungjin, who has been a magnificent friend of my entire life. I would also like to thank my grandmother with all my heart. She raised me when I was a kid and has displayed nothing short of endless love. Her love has always been an enormous encouragement to me. I also deeply acknowledge the kind love of my parents-in-law.

This dissertation is greatly indebted to my baby and wife. With Sooah, my beautiful baby girl, my life has been much more joyous and richer. Soojung, my beloved life partner, has always been with me through the ups and downs of our life. Without her love and assistance, I would not have been able to finish this doctoral study. My deepest and everlasting love to them, and to a baby boy who will soon come to this world.

TABLE OF CONTENTS

Page

Page

Page

LIST OF TABLES

LIST OF FIGURES

Figure Page

ABSTRACT

Choi, Seungmoon. Ph.D., Purdue University, December, 2003. Towards Realistic Haptic Rendering of Surface Textures. Major Professor: Hong Z. Tan.

This dissertation presents a series of studies performed on the perceived instability of haptically-rendered surface textures. By *perceived instability*, we refer to any unrealistic sensations that a user perceives from virtual textures rendered with a force-feedback haptic interface. Our long-term goal is to achieve perceptually realistic haptic rendering of surface textures through a better understanding of factors contributing to perceived instability. Towards this goal, we first quantified the level of perceived stability/instability of a widely-used haptic texture rendering system, and discovered the typical types of perceived instability through psychophysical experiments. Many factors that could potentially affect perceived instability were considered, including texture model parameter, collision detection algorithm, texture rendering method, and human exploration mode. We then characterized the proximal stimuli experienced by a user's hand during the exploration of virtual haptic textures. Several physical variables including position, force and acceleration were measured under conditions where the virtual textures were perceived to be stable and unstable. The proximal stimuli responsible for perceived instability were identified by analyzing measured data in the time and frequency domains, and by comparing the data with known human detection thresholds. Finally, we unveiled the sources of the typical types of perceived instability with additional hypothesis-driven studies based on the measured proximal stimuli. The results of these studies show that (1) the parameter space for perceptually stable haptic texture rendering is too small to be useful for most applications; (2) the typical types of perceived instability (buzzing, aliveness, ridge instability) are due to different characteristics of measured proximal stimuli; (3) a haptic texture rendering system can be passive (therefore stable in the control sense) yet still be perceived as unsta-

ble. This dissertation is among the first to demonstrate that perceived instability can result from both device-control instability and inadequate virtual-environment dynamics modeling. It is argued that significant enhancements in both areas are necessary in order for haptic texture rendering to be widely applicable to real-world applications. Future work will develop better control and environmental modeling algorithms for realistic haptic texture rendering.

1. INTRODUCTION

Haptic rendering is an emerging multidisciplinary scientific area that is concerned with the delivery of object properties to a human user through the sense of *touch*. Owing to the recent developments of sophisticated haptic rendering algorithms running on advanced haptic interfaces, we can now touch virtual objects and feel their properties such as shape, size, and stiffness. Many interesting applications have been developed using the current haptics technology, including surgical simulation, virtual prototyping, and data perceptualization.

One issue that has received increased attention in haptic rendering research community is the addition of *realistic haptic textures* to virtual objects. Haptic objects rendered without surface textures usually feel smooth, and sometimes slippery. Just as visual texture mapping significantly enhances the realism of a graphic scene, haptic textures appropriately superimposed on haptic objects can greatly enrich the sensory attributes of the objects. For example, the same cubic structure can be made to feel like a brick with rough surface textures, or a cardboard carton with finer textures. In order for the field of haptic rendering to reach the next level, it is imperative that haptic texture rendering become more realistic.

Despite the recent progress of haptic texture rendering (see Sec. 2.2 for literature review), many challenges still remain for haptic texture rendering to be widely useful in real-world applications. One problem commonly observed with textures rendered with a force-feedback interface is that of perceived instability. By *perceived instability*, we refer to any unrealistic sensations (such as buzzing and apparent aliveness of a surface) that cannot be attributed to the physical properties of the textures being rendered (see [1] [2] for anecdotal reports of perceived instability). Presence of such perceptual artifacts significantly deteriorates the realism of virtual haptic textures.

This thesis reports a series of studies aimed at a better understanding of perceived instability in haptic texture rendering. Specifically, we have:

- Quantified the level of perceived stability/instability for a widely-used haptic texture rendering system;
- Characterized the proximal stimuli leading to the perception of instability; and,
- Identified sources of perceived instability.

The remainder of this section is organized as follows. In Sec. 1.1, we discuss the concept of perceived instability in depth. Sec. 1.2 outlines the approach that we have taken to accomplish the above three research goals. Finally, the organization of this thesis is laid out in Sec. 1.3.

1.1 Why Perceived Instability?

As illustrated in Fig. 1.1, haptic interaction occurs at an interaction tool of a haptic interface that mechanically couples two controlled dynamical systems: the haptic interface with a computer and the human user with a central nervous system. The two systems are exactly symmetrical in structure and information flow; they sense the environments, make decisions about control actions, and provide mechanical energies to the interaction tool through motions.

Haptic rendering involves three phases. The first phase is the *computation* of force commands using a haptic renderer stored in the computer. This step determines the environment dynamics, the reaction dynamics of the haptic renderer to user movements. In most cases, this environment dynamics is an approximation of the corresponding real-world physics in order to achieve the relatively fast haptic update rate (1 kHz or higher for rendering of rigid haptic objects). This simplified environment dynamics must preserve the essence of the real contact dynamics to produce percepts that are consistent with a user's experience and expectation. Otherwise, the user perceives unrealistic behavior of haptically rendered objects, and perceived instability occurs.

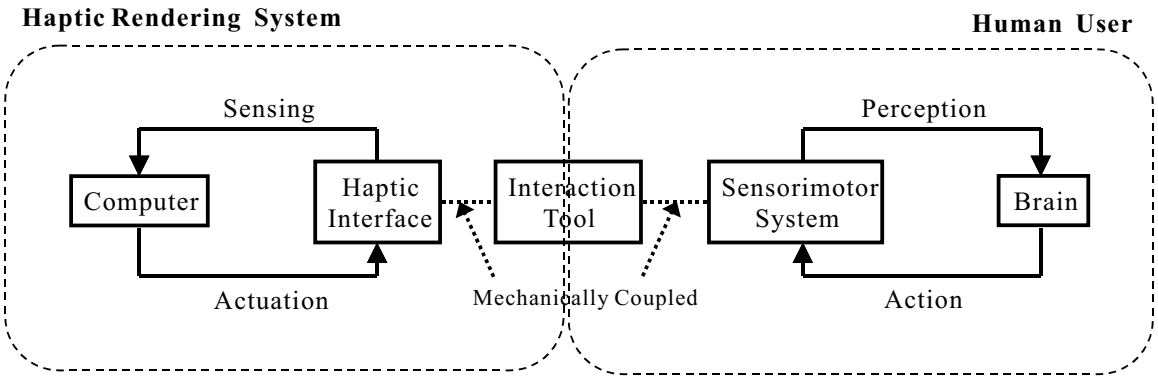

Fig. 1.1. Structure of haptic interaction.

The next phase is the *delivery* of forces to the human user. During this process, the haptic interface has to remain stable in the control sense in order to avoid generating extraneous signals. Device instability may result in perceivable force variations in addition to the force commands received from the haptic renderer.

The final phase of haptic rendering is the *perception* of a haptic scene by a human user. The user perceives the proximal stimuli from the haptic interface, extracts information from the perceived force variations, and forms a percept of the virtual objects being rendered. The user then determines whether the virtual objects feel realistic by comparing the percept to his/her experience of the corresponding real objects. It follows that psychophysical experiments are needed in order to investigate whether a user judges the virtual objects to be realistic.

The status of current research on the three phases of computation, delivery, and perception of forces can be summarized for haptic texture rendering as follows. First, the majority of studies on the development of texture models and rendering techniques have focused on the design of time-efficient computational algorithms (see 2.2 for details). To the best of our knowledge, little attention has been paid to the perceptual validity of such computational methods.

Second, although stable control of a haptic interface has been well studied in the context of control engineering (see Sec. 2.3 for detailed literature review), most studies assume a simple virtual environment such as the "virtual wall". There is an urgent need to extend the techniques for solving the virtual wall stability problem to more complicated domains such as surface textures. Moreover, most studies for stable haptic interaction have been conducted with the implicit assumption that a virtual haptic environment is perceived to be realistic as long as the haptic interface remains stable. The effect of environment dynamics on the realism of a haptic scene is rarely considered.

Finally, few studies have gone beyond the anecdotal observation that stimuli delivered by a haptic interface in a texture rendering system often appear to be unrealistic. Unrealistic sensation of haptically rendered objects is still a new research phenomenon that only occurs in man-made haptic rendering systems. Therefore, psychophysical data concerning the conditions under which perceived instability occurs are not readily available in the literature. To acquire such data requires careful and systematic study of a wide range of haptic texture rendering systems due to the local and sequential nature of haptic perception (in contrast with visual perception that is global and parallel). Since only a small region of an object can be perceived by touch at a time, a user's systematic exploration of the whole object is indispensable in haptic perception in order to detect the presence of any unrealistic sensations with confidence.

In this thesis, we studied *perceived instability* of haptic texture rendering systems to investigate the effects of all components in the haptic interaction loop that can result in unrealistic sensations. In our definition of perceived instability, the user is the ultimate judge on whether stimuli delivered by a force-feedback haptic interface feel realistic. This human-centered concept allows for consideration of all possible sources contributing to perceived instability in a haptic texture rendering system. We have performed a series of studies in order to evaluate a widely-used haptic texture rendering system in terms of perceived instability, and the results are reported in this thesis.

1.2 Our Approach for Analysis of Perceived Instability

The questions that we sought to answer with regard to perceived instability in a haptic texture rendering are three-fold:

- *When* does a user experience perceived instability from haptic virtual textures;
- *What* types of sensations are regarded as perceived instability by a user; and,
- *Why* do such signals exist in a haptic texture rendering system.

To answer the first question, we quantified the conditions under which virtual textures were perceived to be stable or unstable using psychophysical experiments. Various factors were considered in these experiments, including haptic interface, texture model, collision detection algorithm, texture rendering method, and human exploration mode. We also discovered the types of sensations that our subjects judged as unrealistic.

To address the second question, we characterized the proximal stimuli responsible for the perception of the perceived instabilities found in the psychophysical experiments. Several physical variables transmitted through the interaction tool of the haptic interface were measured under various experimental conditions. These conditions were determined based on the results of the psychophysical experiments. The measured data were analyzed by comparing their spectral densities with known human detection thresholds.

Finally, we identified the sources in the haptic texture rendering system that were responsible for generating the proximal stimuli of perceived instability. For each type of perceived instability discovered in the psychophysical experiments, we conducted additional hypothesis-driven experiments to get to its source based on the measured characteristics of the proximal stimuli responsible for its perception.

1.3 Thesis Organization

The remainder of this dissertation proceeds as follows. Ch. 2 provides the background for haptic texture perception and rendering that is needed for understanding this

thesis. Ch. 3 defines the benchmark used throughout this thesis for the analysis of perceived instability during haptic texture rendering. We then report the design and results of the first set of psychophysical experiments performed to quantify the levels of perceived stability/instability for the benchmark in Ch. 4. The measurement experiment conducted to characterize the proximal stimuli of the perceived instability discovered in the psychophysical experiments is discussed in Ch. 5, along with the source of the perceived instability unveiled in the follow-up study. In Chs. 6 and 7, we present the results of another set of psychophysical and measurement experiments in which a different collision detection algorithm was employed. We conclude the thesis in Ch. 8 along with a plan for future work.

2. BACKGROUND

This chapter provides a literature review on haptic texture perception and rendering that can serve as background information for the remainder of this thesis. We begin with a review on the haptic perception of textures and the exploratory actions typically employed for sensing haptic object properties (Sec. 2.1). This is followed by a section on haptic texture rendering (Sec. 2.2). In this section, we discuss the haptic interfaces that have been successfully used for texture rendering and the associated computational methods. The last section (Sec. 2.3) summarizes research on the stable control of haptic interaction and the extensions required for existing methods to be applied to haptic texture rendering.

2.1 Perception and Exploration of Haptic Textures

2.1.1 Perception of haptic textures

Although everyone has some notion of what texture is, the concept of texture is not clearly defined. Katz considered texture as the fine structure of a surface (microstructure), and as independent of the shape (macrostructure) of an object or surface [3]. The systematic study of haptic texture perception began about thirty years ago [4].

One topic that has been controversial in the literature is whether information about surface texture is encoded spatially or temporally. Both types of information are available during direct (fingerpad) exploration, but only temporal cues (vibration) are available during indirect (probe-mediated) exploration. Katz argued that vibration was a necessary condition for texture, particularly roughness, perception [3]. Katz's position was based on the observation that one could easily perceive the roughness of a surface by stroking a pencil across it, and that performance was degraded when the pencil was wrapped in cloth (thereby damping the vibration transmitted through the pencil). Using the fingerpad explo-

ration method, early studies by Lederman and her colleagues argued that vibration served only to prevent the cessation of activity in the mechanoreceptor population [5]. Their experiments found that selective vibrotactile adaptation (which resulted in a change of magnitude estimation of vibration signals) did not alter the perceived roughness of metal gratings [6], and speed of hand movements (which presumably affected the frequency of vibration) barely affected perceived roughness [7]. Consistent with these findings, a spatial-intensive model was proposed for roughness perception based on neurophysiological data [8] [9]. Recently, Lederman and her colleagues have begun to investigate texture perception through the use of intermediate objects such as probes and (compliant or stiff) finger coverings. With the probe-mediated exploration method, a substantial effect of speed was found, thereby supporting a theory based on temporal coding of texture [10] [11].

The consensus that has emerged from these studies is that humans use temporal cues (vibration) while exploring surface textures via a probe. While the same temporal cues are available during fingerpad exploration, humans prefer to use intensive (depth of microstructures) and/or spatial (size of microstructures) cues instead [12]. Performance with bare fingerpad was better for tasks requiring spatial judgments (haptic object recognition), but roughness perception was very similar whether the direct or the indirect method was used [13] [14]. In addition, neurophysiological and psychophysical data suggest that temporal cues are responsible for perception of very fine surface details (with interelement spacing below 1 mm) [15] [16] [17]. For very smooth surfaces, the probe method produced greater perceived roughness than the fingerpad method [18]. Therefore, probe-mediated surface texture perception should yield results similar to the direct method, with better performance expected for very-small-scale (less than 1 mm) surface features.

2.1.2 Exploration of haptic textures

Unlike the visual and auditory senses, the sense of touch is bidirectional. What we perceive about the properties of an object depends on what information we intend to seek and how we expose that information with the way we interact with the object

[19]. Lederman and Klatzky categorized the stereotypical hand movements that people make while exploring object properties and named these movement patterns "Exploratory Procedures (EPs)" [20]. In their study, a total of eight EPs (pressure, lateral motion, static contact, enclosure, unsupported holding, contour following, part motion test, and function test) were discovered and correlated with the specific object properties that the human intends to obtain. They further investigated the relative strengths of the connections between all pairs of EPs and object attributes. These connection strengths are represented by the following four classes of weights [21]:

- Chance: A user is unable to recognize an object attribute with an above-chance accuracy with the EP.
- Sufficient: The recognition accuracy with the EP for an object attribute is above-chance.
- Optimal: The EP is sufficient for perception of an object attribute, and is more accurate and/or faster than any other EP.
- Necessary: The EP is the only one that can produce an above-chance accuracy for an object attribute.

As an example, the weighting of three EPs (pressure, lateral motion, and static contact) and the associated object properties is shown in Table 2.1 [21].

While we are used to using bare hands to manipulate and perceive objects in our daily lives (the direct method), we are limited to using a tool such as a stylus and a gimbal to explore virtual objects rendered with a force-reflecting haptic interface (the indirect method). The range of EPs is limited during indirect exploration, and only the three EPs shown in Table 2.1 are relevant to our study. The other EPs are excluded for the following reasons. First, enclosure EP cannot be performed with a point-contact force-feedback device such as the PHANToM used in the study (see Sec. 3.1). Second, unsupported holding and contour following EPs are not relevant for the virtual environment (i.e., textured surfaces) that this work is concerned with (see Sec. 3.2). Finally, the EPs associated with

Table 2.1
Weighting of exploratory procedures and their effectiveness in revealing certain object properties using bare hands. Shown here are the EPs and object attributes relevant for our study on haptic texture (adapted from [21]).

	Texture	Hardness	Temperature
Pressure	S	O	S
Lateral motion	O	S	S
Static contact	S	C	O

(C: chance, S: sufficient but not optimal, O: optimal but not necessary, and N: necessary.)

Table 2.2
Weighting of exploratory procedures and their effectiveness in conveying certain object properties when a stylus is used.

	Texture	Hardness
Poking	C	O
Stroking	N	S
Static contact	C	C

(C: chance, S: sufficient but not optimal, O: optimal but not necessary, and N: necessary.)

function testing (part motion test and function test) involving multiple-object interaction are not applicable either.

For the remaining three EPs (pressure, lateral motion, and static contact), we can further simplify the associated object attributes shown in Table 2.1 based on the fact that some of the attributes cannot be rendered with a force-feedback device. For example, temperature cannot be displayed with a PHANToM device. This attribute can therefore be removed from Table 2.1. The absence of spatially-distributed information from virtual objects explored with a stylus deprives the pressure and static contact EPs of the texture attribute. Table 2.2 summarizes the relevant EPs and the associated object properties for our study. Note that the names of some EPs are changed to be more descriptive. For haptic exploration with the force-reflecting device, stroking EP is necessary for texture information, and poking is optimal for hardness perception. With static contact EP, a user can only feel the presence of virtual objects.

2.2 Haptic Texture Rendering

2.2.1 Haptic interfaces for texture rendering

As discussed earlier in Sec. 2.1.1, people rely mainly on spatial/intensive cues for texture perception when the bare hand is used. In probe-mediated exploration, however, spatial cues are no longer available. We have to depend solely on temporal cues for texture perception. Therefore, a device that emulates either bare-hand or probe-mediated texture exploration should produce successful rendering of textured surfaces.

Indeed, two types of haptic interfaces have been widely used for texture rendering. One type is a tactile display that is composed of an array of vibratory pins designed to deliver spatiotemporal tactile cues (see [22] [23] [24] [25] for examples of tactile displays). The other type is a force-feedback device that is typically in the form of a joystick or small robotic manipulator with multiple degrees-of-freedom (DoFs). With point contact, a force-feedback device can convey kinesthetic and/or temporal cues, but not spatial cues. Many force-reflecting devices have been developed in the past decade including the

PHANToMs [26], the Delta and Omega devices [27], the Pen-Based Haptic Display [28], and the magnetically levitated force-feedback handle [29] [30].

Force-feedback haptic interfaces are further classified into impedance and admittance displays based on their input-output characteristics [31]. An impedance display is a force-feedback device that measures position and generates force, as opposed to an admittance display that measures force and generates position commands. For the remainder of this section, we restrict our discussion to impedance haptic displays because they are the most common devices and the hardware used in our study (the PHANToM) is of the impedance type.

2.2.2 Principles of haptic rendering

During haptic rendering of virtual scenes with an impedance display such as the PHANToM, the following procedures are carried out repeatedly (See Fig. 2.1 for a flow chart). First, the optical encoders attached to the joints of the PHANToM measure the angles of joint rotations. These joint angles are converted to the position of the stylus tip of the PHANToM in a world coordinate frame using the known kinematics of the PHANToM. Then, the computer determines whether the stylus collides with any of the virtual objects in the database based on the stylus tip position. If a collision is detected, a response force is computed and sent to the user through the PHANToM, in order to convey the perception of the virtual object that the user currently touches. If no collision is detected, no force is exerted so that the user can feel as if he/she is moving in free space. Finally, the database of virtual objects is updated if any information concerning the virtual objects (for example, shapes, positions, and orientations) should be modified due to the interaction.

These rendering procedures are similar to those used for visual simulation of dynamic objects. However, the update rate for haptic rendering is significantly higher than that for visual rendering (30-40 Hz). Slow update rates of rendered force can result in large step changes in force and potentially lead to unstable haptic interaction [32]. Although the

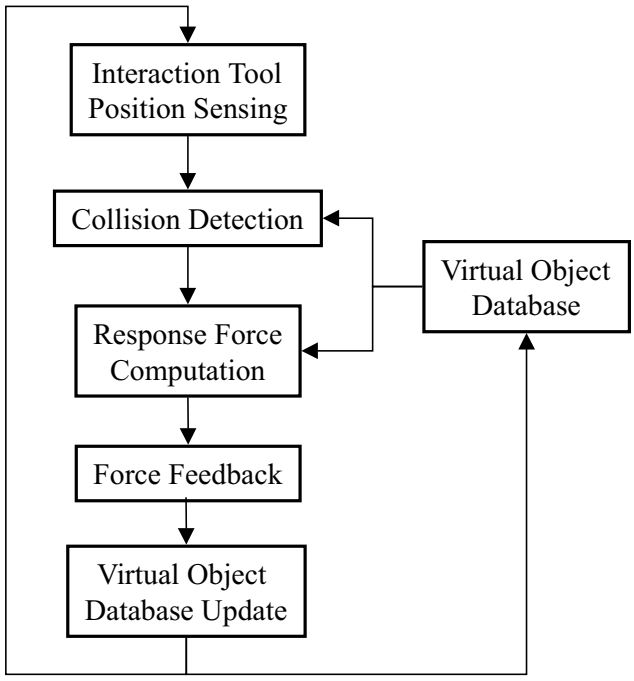

Fig. 2.1. Procedures of haptic rendering with an impedance-type force-reflecting haptic interface.

exact haptic update rate for achieving smooth and stable force rendering depends on applications, the common practice is to use an update rate of 1 kHz or higher for rendering rigid objects. The rendering rate of the PHANToM is set to 1 kHz.

The details of the two computational steps (collision detection and response force computation) for haptic rendering using an impedance display depend on the geometrical models used for virtual objects. The decision on a suitable geometrical model depends on the material property of the virtual objects being considered. In general, there are two classes of mathematical models with respect to this criterion. One class is that of rigid (or solid) objects. The geometry of a solid object is invariant to external force as well as transformation and rotation. Therefore, the internal structure of the rigid object model does not need to be updated during rendering. The other class is that of deformable objects. The structure of a deformable object is subject to change due to external forces, and possibly transformation and rotation (for recent studies, see [33] [34]). Examples of deformable objects include a rubber ball, sponge and human tissues. The model of

a deformable object has to be updated appropriately during haptic interaction, and the computation needed for rendering deformable objects is usually much more complex than that for rigid objects. In this thesis, we are concerned only with rigid textured surfaces (see Sec. 3.2). Therefore, we restrict our further discussion on the methods for response-force computation to those for rigid virtual objects only.

To find a mathematical model of rigid virtual objects, many techniques have been adapted from the more advanced fields of computer graphics and robotics [32]. They include volume methods [26], intermediate plane methods [35] [36], polygonal models [37] [38] [39], and sculpted surfaces [40] [41]. Currently, the polygonal methods dominate the haptic rendering literature due to their simplicity. The relatively simple structure enables fast computation algorithms for contact and depth perception [32]. In our study, we assume that the polygonal model is used to represent a virtual object.

To perform collision detection using virtual objects represented with polygons, the stylus is often represented as a point (the so-called God-object in [37] or the surface contact point in [39]), or an object with simple geometry such as a sphere (the so-called proxy in [38]) in order to facilitate complex geometrical computation. The main ideas in these approaches are that an imaginary point is constrained on the surface of a virtual object with which the stylus is currently in contact, and that the distance between this imaginary point and the actual position of the stylus tip is used as a measure of the penetration depth of the stylus into the surface (See Fig. 2.2). We will refer to this imaginary contact point as the surface contact point following the taxonomy introduced by Ho, et. al. [39].

Once the penetration depth is determined, a resistive force ($\mathbf{f}_{res}(t)$) at time t can be determined using a spring-damper model:

$$\mathbf{f}_{res}(t) = \left[Kd(t) + B\dot{d}(t)\right]\mathbf{n}, \tag{2.1}$$

where $d(t)$ is the penetration depth, $\mathbf{n}$ is the normal vector of the polygon that the stylus is in contact with, and K and B are the stiffness and damping coefficients, respectively. The scenario shown in Fig. 2.2 is referred to as the "virtual wall" problem and has been extensively used as a benchmark for stability studies in haptic rendering.

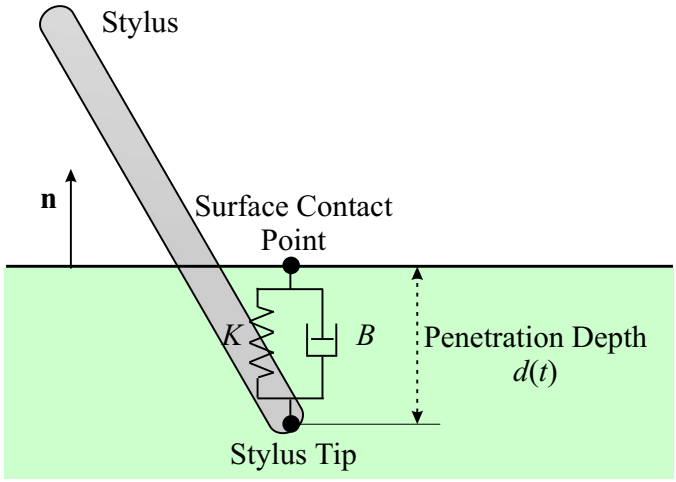

Fig. 2.2. Illustrations of haptic rendering parameters for a rigid plane.

2.2.3 Computational methods for haptic texture rendering

The developments of computational methods for texture rendering have received increased attention from the haptics research community in the past decade. Minsky's Sandpaper system was perhaps the first successful attempt at generating synthetic textures [42] [43]. Using a two DoF force-reflecting joystick, Minsky developed a tangential force-gradient algorithm for two-dimensional texture rendering, where the displayed force is in the plane of the textured surface and proportional to the gradient of the surface-height profile. Several successful implementations of texture rendering methods using three (or more) DoF force-reflecting devices have also been reported. For three-dimensional haptic rendering, resistive forces are rendered to prevent the penetration of an interaction tool into the objects and thus convey the shape (macrogeometry) of virtual objects. To add a sense of surface texture (microgeometry), variations are imposed on these baseline resistive forces. Massie reported that varying the magnitude of the resistive forces alone can generate the perception of textures [44]. Ho, Basodogan and Srinivasan developed more sophisticated texture rendering algorithms by using the bump mapping technique in computer graphics to add perturbations to both the magnitude and direction of the resistive forces for various texture models [39]. Other researchers have used stochastic texture

models [45] [46] [47] [48] and even vibrations superimposed on the resistive forces for haptic texture rendering [49].

These haptic texture rendering techniques use two kinds of texture models (position and force models) to compute the force perturbations that are imposed on the resistive forces for texture information. The position model uses a surface height map to represent the detailed microgeometry of the surface (see, for example, [44] [39]). In a typical implementation of a texture rendering method using the position texture model, the database of virtual objects stores the models of object shape and texture separately. The position texture profile is locally mapped onto a polygon that the user is in contact with via a stylus to construct a textured surface in the response force computation step. The resulting force can then be computed, with an equation similar to Eqn. 2.1, using the penetration depth incorporating the texture height at the surface contact point and the direction vector normal to the textured surface.

The force model adds a force profile to the resistive force directly for texture rendering. Specifically, the response force is computed as

$$\mathbf{f}(t) = \mathbf{f}_{res}(t) + \mathbf{f}_{tex}(t), \tag{2.2}$$

where $\mathbf{f}_{tex}(t)$ is a force vector computed to convey texture information. This force vector can be determined by using either a mathematical function (for example, [45] and [46] use random noises for force perturbations), or a force profile measured from real textures (see, for example, [49] [50]).

Choosing an appropriate texture model for a given application is not a trivial task, but there is little consensus on what texture model is the best one to use in the haptics research community.

2.2.4 Collision detection for haptic texture rendering

In general, the detection of collision between an interaction tool of a haptic interface and virtual objects is a computationally complex and expensive task that has to be executed within a fraction of the haptic update interval. A collision detection problem

is usually reduced to finding a point on an object surface that is closest to the tip of the interaction tool. Many collision detection algorithms for efficient haptic rendering have been studied for general geometrical object models such as polygonal and NURBS models (see [32] for a review).

Haptic textures represented by a force model do not usually require additional computations for collision detection. To calculate a force for texture rendering, one can determine a penetration depth based on the geometrical model for an object shape, compute a resistive force, and then add a force value determined by the force texture model to the resistive force.

However, collision detection becomes much more complex when textures are modeled as positional variations. For simplicity of further discussion, we assume that the shapes of virtual objects are modeled using polygons. Difficulty in collision detection for textured objects arises from two sources. One is the nonlinearity associated with the representation of textured object surfaces. Iterative numerical algorithms are often required to determine a point on a textured surface with a minimum distance from the interaction tool. The computation time required by such an algorithm for a well-converged solution can be too long to be useful for haptic rendering. The other source of difficulty is the lack of a global representation of the boundaries of the textured virtual objects. In a typical implementation, information about the polygons and the texture model are stored separately. The two models are only merged locally, i.e., the texture model is locally mapped onto a point on the polygon for calculating the height and/or perturbed normal at that point. It is often infeasible to search for a global minimum using only the local information.

Few studies have explicitly considered the problem of collision detection in haptic texture rendering, except for that of Ho, Basdogan, and Srinivasan [39]. Their algorithm finds a minimum distance point by using a two-step approach. In the first step, only the polygon information is used. A polygon with a minimum distance from the tip of the interaction tool is determined (for example, polygon L_1 in Fig. 2.3(a)). In the second step, information on both the polygon and the texture model are considered. The distance between the polygon and the tool tip (l) is compared to the height of the texture model

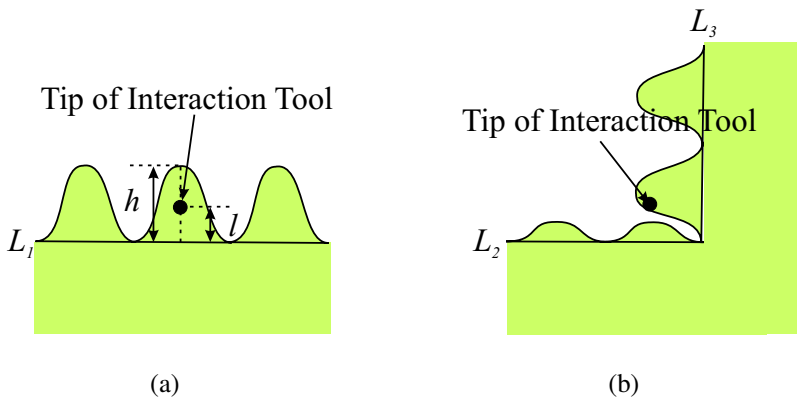

Fig. 2.3. Examples for collision detection of textured virtual objects.

projected on the normal of the polygon (h) to declare an occurrence of collision. This algorithm efficiently makes correct decisions when the tool tip is not too close to the edges of polygons. However, it can fail if the interaction tool is in contact with a bump on another polygon, instead of a bump on top of the polygon found by the minimum distance criterion in the first step. This often happens when the interaction tool is near the edges of polygons, as shown in Fig. 2.3(b). In this case, the tool tip touches a bump on polygon L_3. The algorithm would fail to detect it since polygon L_2 is closer to the tool tip than L_3. To the best of our knowledge, no general solution has been proposed for collision detection in haptic texture rendering.

2.3 Stable Control of Haptic Interaction

A unique challenge to any stability study on haptic rendering using control theory is the fact that haptic interaction occurs between two mechanically coupled dynamic systems: a haptic rendering system (including a haptic interface and a computer) and a human user (including a hand/arm and a central nervous system). The two systems are symmetrical in their structures and information flow (see Fig. 1.1 again). However, they are fundamentally different in the sense that a haptic rendering system is programmed and produces a predictable response to an input, but a human user is volitional and can

react in an unpredictable manner. For instance, the human user can modulate the driving-point mechanical impedance of the hand by changing the muscle activation levels or the postures as she/he desires [51], thereby changing the mechanical load to the haptic interface. This fact suggests that a short-term behavior of a user may be reasonably well modeled to account for the dynamic nature of the human limbs (for example, see [52]), but the long-term response cannot be reliably predicted. A full characterization of the motor commands and mechanical impedance of the human hand/limb is extremely difficult due to the complexity of the human neuromuscular system [53].

Most studies on the stability of haptic interaction have focused on the virtual wall problem that was introduced in Sec. 2.2.2. In this case, the virtual environment to be rendered with a force-feedback device is composed of a plane that does not have any surface details. The objective is to achieve maximum perceived hardness of the wall in a stable manner. The following assumptions are usually made in these studies. First, the haptic interaction is of one-DoF and is perpendicular to the wall. Second, the virtual environment dynamics (the wall) is a mechanical second-order linear system (with stiffness and damping parameters). Third, the contact occurs at a point. Fourth, the force-feedback device has relatively simple dynamics along the direction of penetration (linear dynamics in most cases).

Studies of virtual wall problem usually follow two main directions. One approach is to explicitly model the dynamics of repetitive human motions that are typically observed in haptic interactions and to use the model as plant dynamics. This approach is based on the finding that the dynamics for repetitive human movements often exhibits simple, spring-like behavior to an external environment despite the complexity of the human neuromuscular system [54]. Several studies have modeled the motions of human limbs with second-order linear systems with a high degree of fit (see [52] for example). An example of applying such a typical model of human dynamics to the design of a stable haptic renderer can be found in [51]. However, the robustness of such methods can be problematic with regard to possible rapid changes of the human dynamics model parameters. As a solution to this problem, linear robust control techniques has been applied recently [55].

The other approach uses passivity-based control [56] [31] [57] [58] [59] [60] [61] [62]. It assumes that the human arm is passive when coupled to a passive external system [63], an assumption that finds its support in [64]. A passivity-based analysis does not require the explicit modeling of limb dynamics, and produces a range of rendering parameters that are sufficient for ensuring stable haptic interactions. This novel approach is shown to be useful for many research devices with a relatively large maximum stiffness. However, it tends to result in a conservative parameter range [31]. Therefore, its application to commercially-available haptic interfaces such as the PHANToM [26] may be limited due to the fact that they have relatively small maximum stiffness to begin with.

To the best of our knowledge, no study has tackled the stability of haptic texture rendering using control theory. To do so requires several major extensions to the techniques used for the virtual wall problem, as numerated below. For simplicity, we define a virtual "textured wall" as a single plane with superimposed textures. First, haptic interaction has to be modeled as multi-DoFs because texture is perceived through the variations of physical variables (position and force) that are perpendicular as well as lateral to the wall. Second, the environment dynamics of textured wall problem is much more complex than that of the virtual wall. Textures are often represented with complex nonlinear position or force models as mentioned earlier in Sec. 2.2.3. Computational methods for texture rendering using such texture models behave as highly nonlinear controllers in a haptic rendering system. Third, contacts along a curve need to be considered for the users' stroking motion. Fourth, texture rendering requires force-feedback devices with at least two DoFs. In most cases, interfaces with three or more DoFs and nonlinear dynamics are used. Due to the aforementioned reasons, extending techniques typically used in solving the flat-wall problem to the textured-wall problem will likely lead to a significant increase in the complexity of the theoretical analysis of the stability of a haptic texture rendering system.

3. BENCHMARK

As discussed in the previous chapter, many haptic interfaces and computational algorithms for texture rendering have been developed. For the study of perceived instability of haptic textures, we decided to choose a haptic texture rendering system that includes essential features common to many existing haptic interfaces and computational algorithms. It was also necessary to consider the effects of user actions during the exploration of virtual textured objects. This chapter introduces the benchmark used for the study of perceived instability throughout this thesis.

3.1 Apparatus

We used the PHANToM (Sensable Technologies, Woburn, MA; model 1.0A) to render virtual textured surfaces for our study (see Fig. 3.1 for a picture), as it is one of the most widely used devices for haptic research and applications. The PHANToM is a serial-linkage manipulator with three revolute joints for three-dimensional force generation, and three optical encoders (one at each joint) for position sensing. This PHANToM model has a nominal position resolution of 0.03 mm and a nominal maximum stiffness of 3.5 N/mm. A gimbal or stylus can be attached at the wrist of the PHANToM as an interaction tool to be grasped by a user to perceive virtual objects. Our model of PHANToM has three additional encoders at the wrist to sense the orientation of the interaction tool. The stylus was used as the interaction tool in all experiments reported in this thesis.

3.2 Texture Model

The virtual textured surfaces were modeled as one-dimensional (1D) sinusoidal gratings superimposed on a flat surface. This underlying flat surface, defined by $z = 0$ in

Fig. 3.1. PHANToM force-feedback haptic interface (model 1.0A).

the world coordinate frame of the PHANToM, formed a vertical wall facing the user of the PHANToM (see Fig. 3.2). The sinusoidal grating was described by $z = A\sin(\frac{2\pi}{L}x) + A$, where A and L denote the amplitude and (spatial) wavelength, respectively (see Fig. 3.3). Sinusoidal gratings have been widely used as the basic building blocks for textured surfaces for studies on haptic texture perception [11] [2]. They have also been used as a basis function set for modeling real haptic textures [65].

3.3 Collision Detection

We considered two methods for penetration depth computation defined as follows:

$$d_1(t) = \begin{cases} 0 & \text{if } p_z(t) > 0 \\ A\sin\left(\frac{2\pi}{L}p_x(t)\right) + A - p_z(t) & \text{if } p_z(t) \leq 0 \end{cases}, \quad \text{and} \tag{3.1}$$

$$d_2(t) = \begin{cases} 0 & \text{if } p_z(t) > h(p_x(t)) \\ A\sin\left(\frac{2\pi}{L}p_x(t)\right) + A - p_z(t) & \text{if } p_z(t) \leq h(p_x(t)) \end{cases}, \tag{3.2}$$

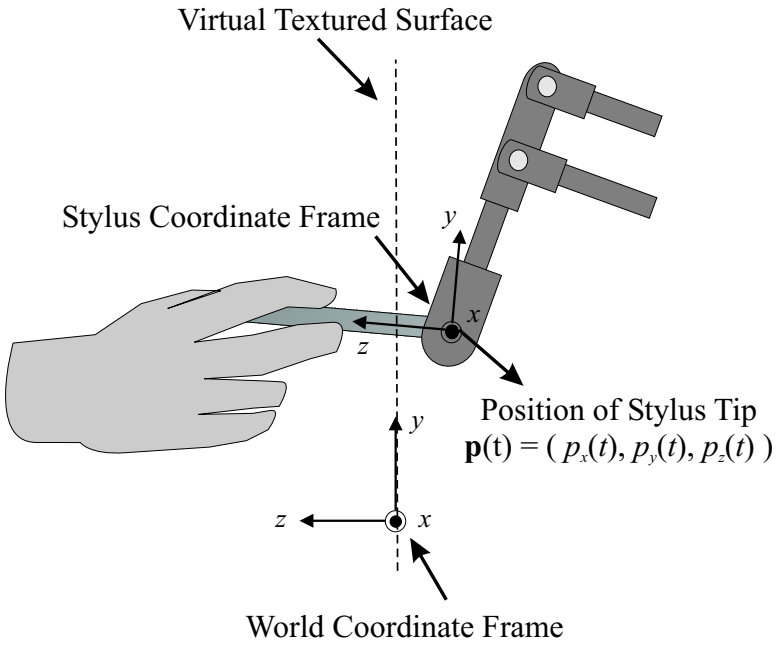

Fig. 3.2. An illustration of the virtual textured surfaces and the two coordinate frames used in our experiments. Position of the stylus tip was always measured in the world coordinate frame.

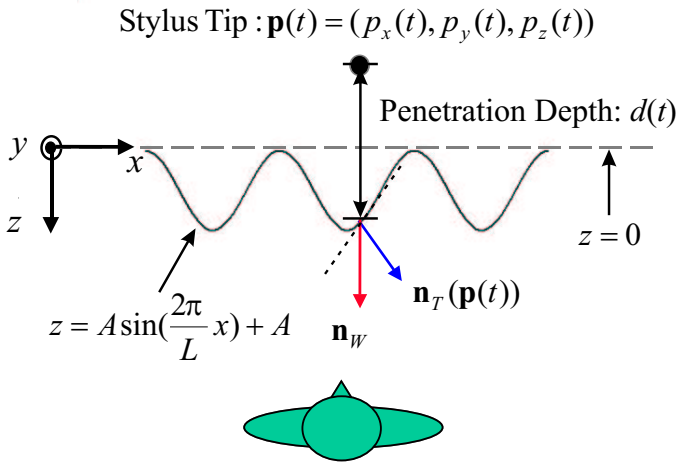

Fig. 3.3. An illustration of the parameters used in texture rendering.

where $\mathbf{p}(t) = (p_x(t), p_y(t), p_z(t))$ is the position of the PHANToM stylus tip, and $h(p_x(t)) = A\sin\left(\frac{2\pi}{L}p_x(t)\right) + A$ is the height of the texture model at $p_x(t)$.

The first method $d_1(t)$ assumes that the collision detection is based on the plane underlying the textured surface ($z = 0$). Since this plane represents a face of a polygon, $d_1(t)$ can be easily generalized to textured objects with a large number of underlying polygons. However, it introduces discontinuities in the computed penetration depths when the PHANToM stylus enters and leaves the textured surfaces.

The second method $d_2(t)$ declares a collision as soon as the stylus enters the texture boundary. This method ensures a continuous change in the computed penetration depths. However, it is much more difficult to apply this algorithm to textured objects with arbitrary shapes due to the reasons discussed in Sec. 2.2.4.

3.4 Texture Rendering Method

We examined two basic texture rendering methods in this thesis. Both methods use a spring model to calculate the magnitude of rendered force as $K \cdot d(t)$, where K is the stiffness of the textured surface, and $d(t)$ (= either $d_1(t)$ or $d_2(t)$) is the penetration depth of the stylus at time t (see Fig. 3.3).

The two methods differ in the way the force directions are rendered. The first method, introduced by Massie [44], renders a force $\mathbf{F}_{mag}(t)$ with a constant direction normal to the underlying flat wall of the textured surface. The second method, proposed by Ho, Basdogan and Srinivasan [39], renders a force $\mathbf{F}_{vec}(t)$ with varying directions such that it remains normal to the local micro-geometry of the sinusoidal texture model. Mathematically,

$$\mathbf{F}_{mag}(t) = K\,d(t)\,\mathbf{n}_W, \tag{3.3}$$

$$\mathbf{F}_{vec}(t) = K\,d(t)\,\mathbf{n}_T(\mathbf{p}(t)), \tag{3.4}$$

where $\mathbf{n}_W$ is the normal vector of the underlying flat wall, and $\mathbf{n}_T(\mathbf{p}(t))$ is the normal vector of the textured surface at $\mathbf{p}(t)$. Both methods keep the force vectors in the horizontal plane (zx plane in Fig. 3.2), thereby eliminating the effect of gravity on rendered forces.

The two texture rendering methods are natural extensions of virtual flat wall rendering techniques. Perceptually, they are very different: textures rendered by $\mathbf{F}_{vec}(t)$ feel rougher than those rendered by $\mathbf{F}_{mag}(t)$ for the same texture model. Textures rendered by $\mathbf{F}_{vec}(t)$ can also feel sticky sometimes.

3.5 Exploration Mode

We tested two exploration modes: free exploration and stroking, to examine the effect of user interaction patterns on instability perception. In the free exploration mode, subjects were allowed to use the interaction pattern that they found most effective at discovering instability of virtual textures. This mode was selected to be the most challenging interaction pattern for a haptic texture rendering system in terms of perceived instability. In the stroking mode, subjects were instructed to move the stylus laterally across the textured surface (i.e., along the x axis as shown in Fig. 3.2). Stroking is the exploration mode most frequently employed by humans for texture perception and identification as mentioned earlier in Sec. 2.1.2.

4. QUANTIFICATION OF PERCEIVED INSTABILITY: PART I

[1]To investigate perceived instability of a haptic texture rendering system defined in the previous chapter, we first conducted psychophysical experiments for a quantitative analysis of perceived instability. The specific objectives of these experiments were 1) to quantify the parameter space for perceptually stable haptic virtual textures, and 2) to gather qualitative descriptions of different kinds of perceived instability.

We report the design and results of the first part of our psychophysical experiments in this chapter. These experiments used a collision detection algorithm based on $d_1(t)$ in Eqn. 3.1. The second part of our psychophysical experiments, where a collision detection algorithm based on $d_2(t)$ in Eqn. 3.2 was used, will be presented in Ch. 6.

4.1 Experiment Design

4.1.1 Apparatus

The PHANToM force-reflecting haptic interface was used in all experiments to render virtual textured surfaces.

4.1.2 Stimuli

The virtual texture models used in the experiments had two parameters, amplitude A and wavelength L of the 1D sinusoidal gratings. Three values of A (0.5, 1.0, and 2.0 mm) and three values of L (1.0, 2.0, and 4.0 mm) were tested, resulting in a total of nine textured surface profiles. These sinusoidal gratings can be well constructed due to the 0.03

[1]The materials presented in Chs. 4 and 5 will appear in S. Choi and H. Z. Tan, "Perceived Instability of Virtual Haptic Texture. I. Experimental Studies," *Presence: Teleoperators and Virtual Environments*, Cambridge, MA: The MIT Press, in press.

mm nominal positional resolution of the PHANToM (see Sec. 3.1). Each surface profile was rendered with the two texture rendering methods described in Eqns. 3.3 and 3.4 using $d_1(t)$ for $d(t)$ and stiffness K as the parameter. It follows that the three parameters, A, L, and K, along with the texture rendering methods, uniquely defined the stimuli used in this study.

Due to the fact that the PHANToM workspace boundary exhibits inferior dynamics performance, the virtual textured surface was restricted to a 15cm $\times$ 15cm region located near the center of the PHANToM workspace.

4.1.3 Subjects

Three subjects participated in these experiments. One subject (S1, male) was an experienced user of the PHANToM haptic interface. The other two subjects (S2 and S3, females) had not used any haptic interface prior to this study. The average age of the subjects was 26.3 years old. All subjects are right-handed and reported no known sensory or motor abnormalities with their upper extremities.

4.1.4 Conditions

The independent variables employed in the experiments were texture rendering method, exploration mode, and amplitude and wavelength values of sinusoidal surface profiles. Four experiments, defined by the combinations of the two texture rendering methods and the two exploration modes, were conducted. There were nine conditions (3 A $\times$ 3 L values) per experiment (see Table 4.1).

The dependent variable measured in all 36 experimental conditions (4 experiments $\times$ 9 conditions per experiment) was the maximum stiffness K below which the rendered textured surface was perceived to be stable.

Table 4.1
Experimental conditions for psychophysical experiment using $d_1(t)$.

Experiment	Texture Rendering Method	Exploration Mode	A (mm)	L (mm)
I-1	$\mathbf{F}_{mag}(t)$	Free Exploration	0.5, 1.0, 2.0	1.0, 2.0, 4.0
I-2	$\mathbf{F}_{mag}(t)$	Stroking	0.5, 1.0, 2.0	1.0, 2.0, 4.0
I-3	$\mathbf{F}_{vec}(t)$	Free Exploration	0.5, 1.0, 2.0	1.0, 2.0, 4.0
I-4	$\mathbf{F}_{vec}(t)$	Stroking	0.5, 1.0, 2.0	1.0, 2.0, 4.0

4.1.5 Procedure

All subjects went through initial training to develop criteria for the perception of instability of a virtual textured surface. During the training, the subject chose the texture rendering method and selected the values of A, L and K. The subject was informed that the virtual textures were rendered as 1D sinusoidal gratings. The subject was instructed to regard any sensation that felt unrealistic based on her/his experience of real textures as an indication of perceived instability. Each subject spent approximately one hour on training.

The method of limits [66] was used in all experiments. Given a pair of A and L values within each of the four experiments, a total of 100 series of trials (50 ascending series and 50 descending series) were conducted. Each ascending series started with a stiffness value of $K_{min} = 0.0$ N/mm (i.e., no force) that was always perceived to be stable. The subject would respond "stable" (by pressing a designated key on the keyboard). The K value was then increased by $\Delta K = 0.02$ N/mm. The subject would feel the virtual textured surface again and respond "stable" or "unstable" according to the perception. As long as the subject chose to report "stable", the K value was incremented by the same ΔK amount for each subsequent trial. An ascending series was terminated when the subject reversed the response from "stable" to "unstable." The value of $K + \Delta K/2$ was then recorded as

the estimated threshold for this ascending series, where K was the stiffness of the last trial with a "stable" response.

Each descending series started with a stiffness value of $K_{max} = 0.6$ N/mm. This value was selected based on the preliminary finding that no textured surface felt stable at this K value. The same step size of $\Delta K = 0.02$ N/mm was used to decrease K values in each subsequent trial. A descending series was terminated when the subject reversed the response from "unstable" to "stable." The value of $K - \Delta K/2$ was then recorded as the estimated threshold for this descending series, where K was the stiffness of the last trial with an "unstable" response. With these chosen values of K_{min}, K_{max} and ΔK, each ascending/descending series could last up to 31 trials.

The experiments proceeded as follows. Each subject performed all nine conditions (3 A values $\times$ 3 L values) in Exp. I-1 first, followed by those in Exps. I-2, I-3, and I-4. The order of the nine conditions within each experiment was randomized for each subject. For each pair of A and L values, the order of the 50 ascending and 50 descending series was also randomized.

During all experiments, subjects wore headphones with white noise to block the auditory cues emanating from the PHANToM. No visual rendering of the textured surface was provided. Instead, the computer monitor displayed only text information on the current series number.

The following instructions were given to the subjects during all experiments. They were asked to hold the stylus lightly, and to hold it like a pencil. For the free exploration mode (Exps. I-1 and I-3), the subjects were asked to detect any sensations indicating instability using whatever interaction style they had chosen. For the stroking mode (Exps. I-2 and I-4), the subjects were instructed to concentrate on the detection of sensations indicating instability while they moved the stylus back and forth along the x direction across the textured surface. They were asked to maintain a constant stroking velocity to the best of their ability.

Typically, it took about an hour for a subject to finish one experimental condition. Each subject finished two or three experimental conditions per day. It took a total of ap-

proximately 36 hours for each subject to complete the 36 experimental conditions. A ten-minute break was enforced after a subject had completed the 100 ascending/descending series associated with one experimental condition. This was necessary in order to prevent a carryover effect (i.e., surfaces presented after a series of particularly unstable conditions might have been judged as more stable in a subsequent experiment). Subjects were also allowed to take a break whenever it was needed.

4.1.6 Stability of nontextured flat wall

After the completion of the main experiments, one subject (S1) was tested with a nontextured flat wall using the same procedure as described above. The result of this test served as a baseline value for stiffness K.

4.2 Results

As discussed earlier, 50 ascending and 50 descending series were conducted for each experimental condition (i.e., each pair of A and L values within a main experiment). Fig. 4.1 shows typical results for one experimental condition (subject S1, $\mathbf{F}_{mag}(t)$, stroking, A=2.0 mm, L=2.0 mm). The top panel shows the histogram for all 50 ascending series, the middle panel for all 50 descending series, and the bottom panel for combined series. The average of K values from the 50 ascending series (0.26 N/mm) was greater than that from the descending series (0.19 N/mm). This is typical and reflects what is termed the "errors of habituation" [66]. It is a common practice to compute the mean from the combined data (0.23 N/mm) and regard it as an estimate of the stiffness threshold, K_T.

Results from Exp. I-1 ($\mathbf{F}_{mag}(t)$, free exploration) are shown in Fig. 4.2 for the three subjects in separate panels. In each panel, the stiffness thresholds are indicated by squares at their respective A and L values. The mesh shows the fitted surface computed by linear regression analysis (see Eqn. 4.1 later). To help the reader visualize the spatial relationship between threshold data points (squares) and the fitted surface (mesh), straight lines are drawn between the centers of data points and the corresponding points on the

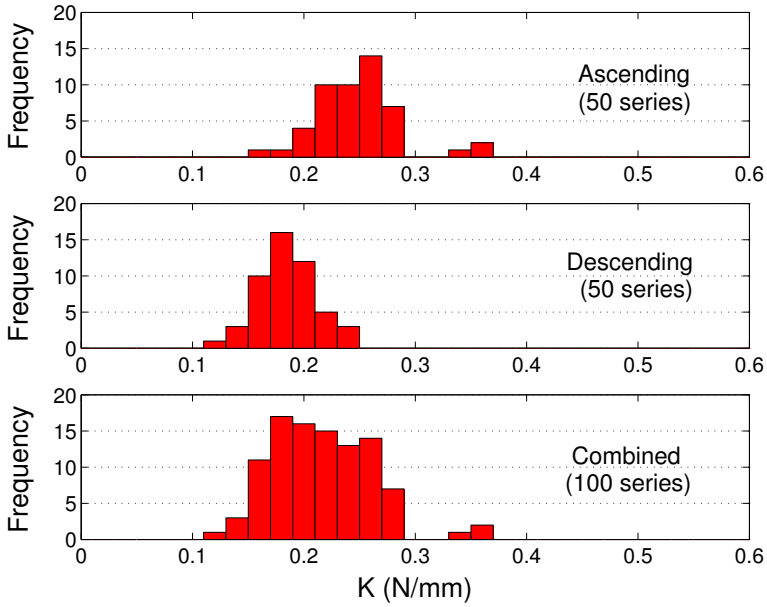

Fig. 4.1. Typical histograms for one experimental condition (Exp I-2, subject S1, A=2.0 mm, L=2.0 mm) using the method of limits.

mesh with the same A and L values. The standard errors are not indicated in the figures because they were very small (the average standard error was 0.004 N/mm). The volume under the mesh represents the parameter space within which all virtual textured surfaces were perceived to be stable. As can be seen from Fig. 4.2, these volumes were quite small for all subjects. Subject S2 produced the largest volume for stable texture rendering and S3 the smallest. Recall that subject S1 was the only one who was experienced with the PHANToM device. Therefore, prior experience with a force-reflective haptic interface did not necessarily result in a particularly stringent or lenient criterion for judging the stability of virtual textured surfaces.

A five-way ANOVA analysis (subject, texture rendering method, exploration mode, A, and L) showed that there were significant differences among the three subjects tested ($F(2,10791) = 484.57,\ p < 0.0001$). However, since all three plots in Fig. 4.2 exhibited the same general trends, data from all subjects were pooled and summarized in panel (a) of Fig. 4.3. Also shown in Fig. 4.3 are the results from Exps. I-2 (panel (b)), I-3

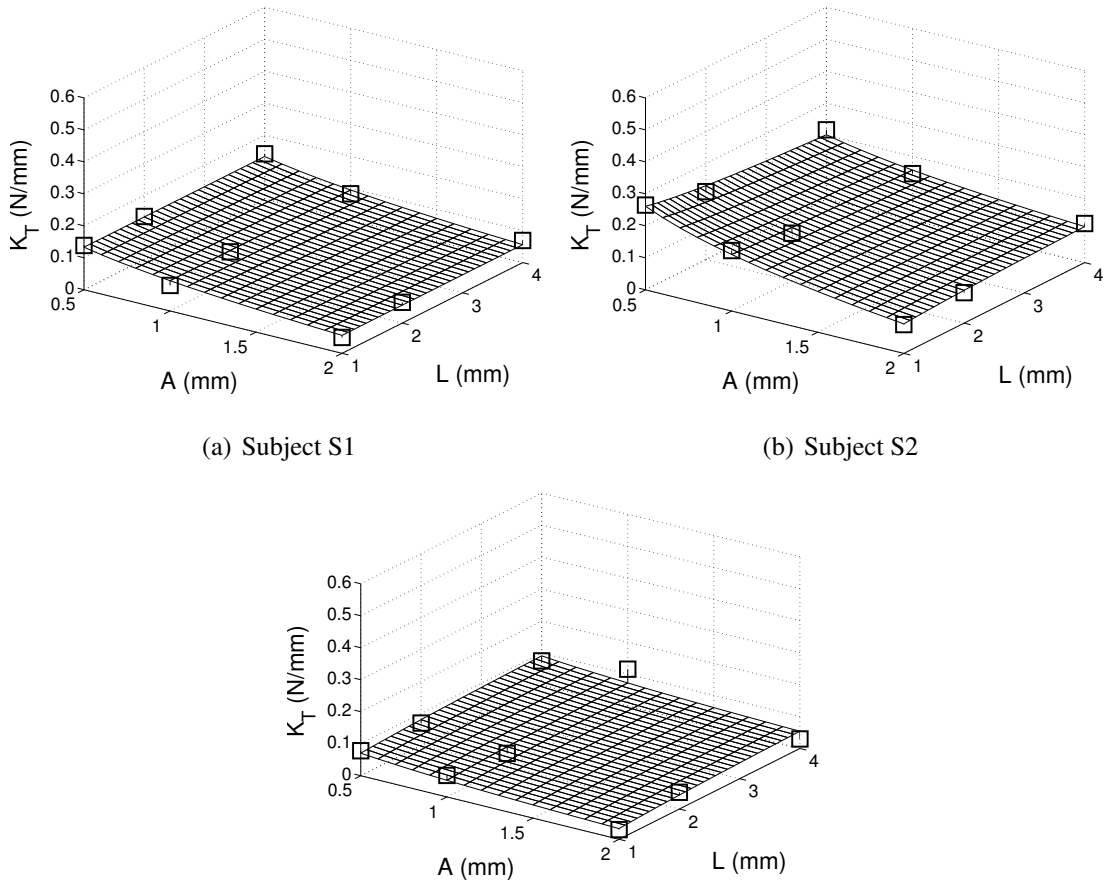

(a) Subject S1

(b) Subject S2

(c) Subject S3

Fig. 4.2. Experimental results of Exp. I-1 for all subjects. The stiffness thresholds K_T are indicated by squares. Regression surfaces representing the boundary of K_T for perceptually stable texture rendering are also shown. A solid line is drawn between the center of a datum point and the corresponding point on the regression surface with the same A and L values to help visualize the position of the datum point.

(panel (c)) and I-4 (panel (d)). Overall, the values of K_T ranged from 0.0138 N/mm to 0.4527 N/mm for all the conditions tested. These values were quite small and the resulting textured surfaces felt very soft (like corduroy). They were also much smaller than the stiffness threshold measured with a nontextured wall (1.005 $\pm$ 0.157 N/mm for subject S1). The effect of exploration mode can be observed by comparing panel (a) with (b) and (c) with (d). The thresholds associated with the stroking mode (panels (b) and (d)) were larger than those associated with the free-exploration mode (panels (a) and (c)) by an average difference of 0.137 N/mm ($F(1,10764) = 5980.13$, $p < 0.0001$). The thresholds for surfaces rendered with the $\mathbf{F}_{\text{mag}}(t)$ method (panels (a) and (b)) were statistically greater than those with the $\mathbf{F}_{\text{vec}}(t)$ method (panels (c) and (d)) by an average difference of 0.099 N/mm ($F(1,10764) = 3103.44$, $p < 0.0001$).

The functional relationship between (A, L) and K_T were estimated using the following form of a fitted equation:

$$\hat{K}_T = \beta_0 + \beta_A \log_2 A + \beta_L \log_2 L + \beta_{AL} \log_2 A \cdot \log_2 L. \tag{4.1}$$

The estimated coefficients are listed in Table 4.2 for all experiments. They were computed by linear regression analysis for K_T with two log-scaled continuous variables ($\log_2 A$ and $\log_2 L$) and two categorical variables (texture rendering method and exploration mode) as well as their interaction terms ($R^2 = 0.5908$; R^2 is relatively small because we pooled the data of three subjects whose results were significantly different). Note that the nonsignificant coefficients are set to zero in this table.

The effects of the amplitude (A) and wavelength (L) of the sinusoidal gratings on the stiffness threshold K_T can be observed from Fig. 4.3 and Table 4.2. In Exps. I-1 and I-2, it is evident from Fig. 4.3 that K_T decreased as A increased. The wavelength (L) had an effect on K_T only through the interaction term $\log_2 A \cdot \log_2 L$, but its effect was very small compared to that of A ($\beta_L = 0.0$, $|\beta_{AL}| \ll |\beta_A|$). In Exp. I-3 and I-4, increasing A or L tended to result in lower or higher K_T, respectively, unless K_T was very small, and their interaction was more apparent ($|\beta_{AL}|$ of Exps. I-3 and I-4 $\gg |\beta_{AL}|$ of Exps. I-1 and I-2).

Subject debriefing revealed several types of perceived instability during haptic texture rendering. In the free exploration mode, subjects reported that they perceived three

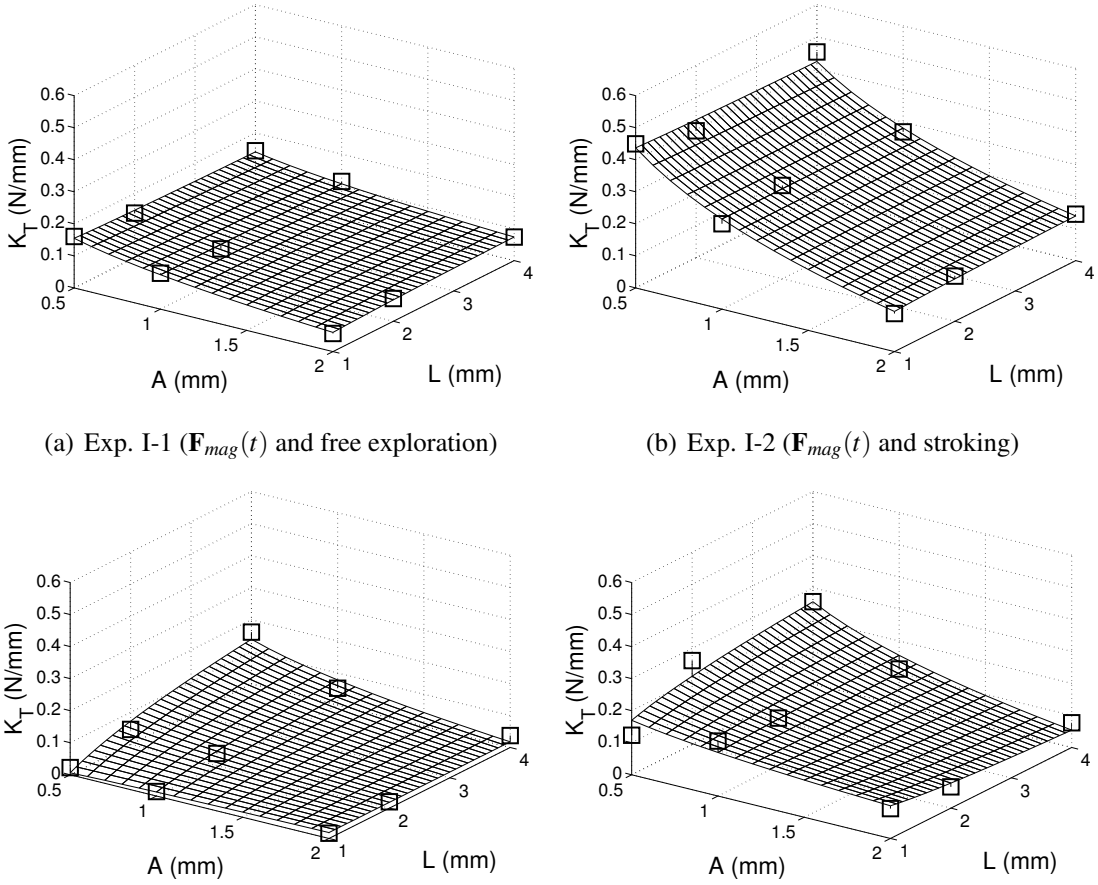

(a) Exp. I-1 ($\mathbf{F}_{mag}(t)$ and free exploration)

(b) Exp. I-2 ($\mathbf{F}_{mag}(t)$ and stroking)

(c) Exp. I-3 ($\mathbf{F}_{vec}(t)$ and free exploration)

(d) Exp. I-4 ($\mathbf{F}_{vec}(t)$ and stroking)

Fig. 4.3. Results of psychophysical experiments using $d_1(t)$. The stiffness thresholds averaged over all three subjects are shown with open squares. Regression surfaces representing the boundary of K_T for perceptually stable texture rendering are shown with meshes. To help the reader visualize the position of the data, a solid line is drawn between the center of each datum point and the corresponding point on the regression surface with the same A and L values.

Table 4.2
Coefficients of fitted regression equation.

Experiment	β_0	β_A	β_L	β_{AL}
I-1	0.107	-0.048	0.0	0.007
I-2	0.281	-0.156	0.0	0.007
I-3	0.012	0.007	0.033	-0.033
I-4	0.136	-0.034	0.010	-0.033

types of apparent instabilities: *entry instability*, *inside instability*, and *ridge instability*. These terms reflect the position of the stylus tip where the corresponding type of instability was perceived. Entry instability refers to the phenomenon that as the stylus approached a point on the $z = 0$ plane (see Fig. 3.3), a high-frequency buzzing of the stylus sometimes occurred. Inside instability was frequently associated with the action of poking. It was most evident when the stylus was pushed deep into a virtual textured surface rendered with $\mathbf{F}_{vec}(t)$. Ridge instability occurred when the stylus was pushed by the PHANToM into the valley of a sinusoidal grating while the subject tried to maintain its position on a ridge of the grating. The subjects also reported that entry and inside instabilities were more pronounced than ridge instability, and therefore they mainly focused on the first two types of instability. In the stroking mode, the textured surface was perceived to be unstable when the subject felt a buzzing noise in addition to the vibrations resulting from the sinusoidal gratings being stroked across.

4.3 Discussion

In the psychophysical experiments, we measured the parameter space within which the subjects did not perceive any instability associated with the virtual textures. We tested two texture rendering methods using sinusoidal gratings and two exploration modes. The maximum stiffness values under which no instability was perceived turned out to be in the

range of 0.0138 to 0.4527 N/mm. This range corresponded to surfaces that were soft and spongy to the touch. The stiffness threshold was much smaller than that of a flat surface with no texture (1.005 N/mm).

Our finding that stroking resulted in a larger stiffness threshold than free exploration for the same rendering parameters is to be expected. We recall that our subjects rarely used stroking in the free exploration mode although it was allowed. Instead, they chose to position the stylus at various locations on or inside the virtual textured surface to focus on the detection of any buzzing as an indication of instability. Therefore, in the free exploration mode, the subjects concentrated on the detection of vibrations in the absence of any other signals. In the stroking mode, the subjects always felt the vibration due to the stylus stroking the virtual textured surface. They had to detect *additional* noise in order to declare the textured surface to be unstable. Due to possible masking of buzzing noise by the vibrations coming from the textured surface, it is conceivable that subjects were not able to detect instability with stroking as easily as they could with static positioning of the stylus (free exploration). In fact, the subjects reported that the experiments with stroking were more difficult to perform. Therefore, textured surfaces explored by stroking appeared to be more stable than those explored by poking or static contact.

Our finding that textures rendered with $\mathbf{F}_{mag}(t)$ resulted in a larger stiffness threshold than those rendered with $\mathbf{F}_{vec}(t)$ is also consistent with the nature of these two rendering methods. While $\mathbf{F}_{mag}(t)$ imposed perturbations in the magnitudes of rendered forces only, $\mathbf{F}_{vec}(t)$ resulted in perturbations in both the directions and the magnitudes of rendered forces. The sometimes abrupt changes in force direction could cause virtual textures rendered with $\mathbf{F}_{vec}(t)$ to be perceived as less stable than those rendered with $\mathbf{F}_{mag}(t)$. To circumvent this problem, Ho, Basdogan, and Srinivasan, who originally proposed the $\mathbf{F}_{vec}(t)$ rendering method, have developed a heuristic algorithm that interpolates the direction of a force vector between the normal to the texture model and that to the underlying surface [39].

To gain intuition into the effects of A or L on K_T, we consider the derivative of the magnitude of the rendered force. Let $g(t) = \left|\mathbf{F}_{mag}(t)\right| = |\mathbf{F}_{vec}(t)|$, and assume that the stylus is in contact with the textured surface. From Eqns. 3.1, 3.3, and 3.4, we have

$$g(t) = K\left[A\sin\left(\frac{2\pi}{L}p_x(t)\right) + A - p_z(t)\right].$$

Differentiating $g(t)$ with respect to the time variable t results in

$$\dot{g}(t) = 2\pi\frac{KA}{L}\cos\left(\frac{2\pi}{L}p_x(t)\right)\dot{p}_x(t) - K\dot{p}_z(t). \tag{4.2}$$

There are two terms in this equation that determine the rate of change in the force magnitude. The term on the right, $K\dot{p}_z(t)$, responds to stylus motion in a direction that is normal to the underlying plane ($\dot{p}_z(t)$) with a gain of K. This is the same term that has been used in formulating the virtual wall (with no texture) problem. The term on the left is due to textures on the virtual wall. Here, the lateral velocity of the stylus ($\dot{p}_x(t)$) is amplified with three constant gains (K, A, and $1/L$) and one variable gain that depends on the stylus position in the lateral direction ($p_x(t)$). Increasing A or decreasing L results in a faster change in force magnitude which can cause a textured surface to be perceived as less stable, or equivalently, result in a smaller stiffness threshold K_T.

Of the three types of instability discovered by the subjects, the sensation associated with entry and inside instability was that of buzzing and vibration. The entry instability was commonly observed for both texture rendering methods. This instability may have resulted from the collision detection algorithm used in the experiments. The collision detection algorithm declares a collision when the PHANToM stylus enters the underlying plane. Thus, the penetration depth computed following Eqn. 3.1 included step changes when the stylus entered and left the texture plane, and these step changes may have caused the perception of inside instability. Despite this known problem, this collision detection algorithm is a basic and useful method that can be easily generalized to complex textured objects as discussed earlier in Sec. 3.3.

The inside instability frequently observed in textures rendered with $\mathbf{F}_{vec}(t)$ seems to be consistent with the nature of the texture rendering method. When the stylus is posi-

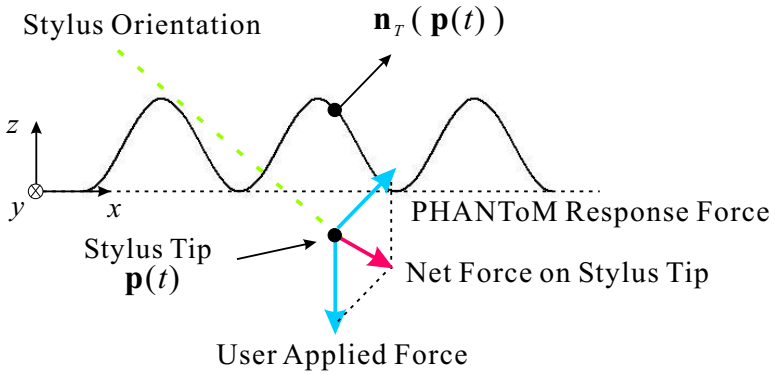

Fig. 4.4. An illustration of the forces involved in ridge instability.

tioned deep inside the texture surface, $\mathbf{F}_{vec}(t)$ generates forces with relatively large magnitudes and fast direction changes. This may have invoked the generation of high-frequency signal that the subjects described as buzzing.

The sensation associated with ridge instability was qualitatively different and was likely due to the environment model of the textured surface. When a real stylus rests on the ridge of a real surface with sinusoidal gratings, the reaction force and friction of the surface combine to counterbalance the force exerted by the user's hand on the stylus, thereby creating an equilibrium. The force rendered by $\mathbf{F}_{vec}(t)$, however, was determined solely on the local texture geometry and did not take into account the direction of user applied force. This is illustrated in Fig. 4.4, where it is assumed that the force applied by the user was normal to the plane underneath the texture. According to the environment model, the force applied by the PHANToM was always in the direction of the surface normal $\mathbf{n}_T(\mathbf{p}(t))$. As a result, the net force exerted on the tip of the stylus (the sum of the forces applied by the user and the PHANToM) was directed towards the valley of the sinusoidal grating. Therefore, the subject who tried to rest the stylus on the ridge could feel the stylus being actively pushed into the valley.

In summary, the results of the psychophysical experiments showed that the parameter space for stable texture rendering was too limited to be useful for virtual environment applications or psychophysical studies. As mentioned earlier, the textured surfaces within the stable rendering-parameter range felt like soft corduroy. We were not able to render harder or rougher textured surfaces without inducing the perception of instability. It was therefore necessary to investigate the characteristics and sources of signals that gave rise to perceived instability, with the goal to eliminate them in order to increase the useful parameter space for stable texture rendering.

5. CHARACTERIZATION OF PROXIMAL STIMULI: PART I

[1]In this chapter, we present the results on the measurement of the proximal stimuli (position of the tip of the stylus, force, and acceleration) delivered to a subject's hand during the exploration of virtual textures. The specific objectives of this experiment were: 1) to isolate signals responsible for perceived instability; 2) to identify the signal components responsible for the perception of texture and instability, respectively; 3) to analyze the intensity of the proximal stimuli in both physical and perceptual units, and 4) to investigate the sources of signals causing the perception of instability. For all experimental conditions reported in this chapter, $d_1(t)$ in Eq. 3.1 was used for penetration depth computation. Measurement studies using $d_2(t)$ will appear later in Ch. 7.

5.1 Experiment Design

5.1.1 Apparatus

The PHANToM force-reflecting device was used for both texture rendering and data collection. The position of the tip of the stylus, $\mathbf{p}(t)$, was measured using the position sensing routines in the GHOST library provided with the PHANToM. These routines read the optical encoders to sense joint angles of the PHANToM and converted them to a position of the stylus tip in the world coordinate frame.

For force and acceleration measurement, the PHANToM was instrumented with two additional sensors. A triaxial force/torque (F/T) sensor (ATI Industrial Automation, Apex, NC; model Nano17 with temperature compensation) was used to measure force delivered by the PHANToM, $\mathbf{f}(t)$. In order to minimize the structural change to the PHAN-

[1]The materials presented in Chs. 4 and 5 will appear in S. Choi and H. Z. Tan, "Perceived Instability of Virtual Haptic Texture. I. Experimental Studies," *Presence: Teleoperators and Virtual Environments*, Cambridge, MA: The MIT Press, in press.

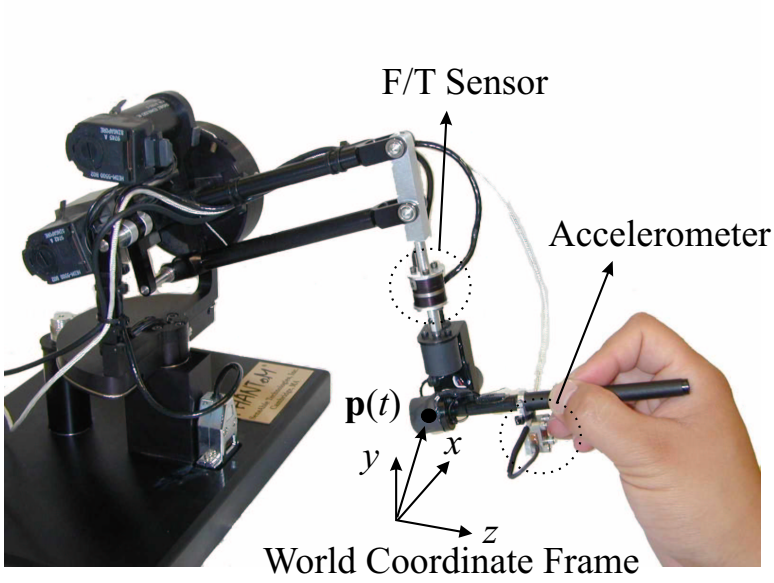

Fig. 5.1. The PHANToM instrumented with a triaxial F/T sensor and an accelerometer.

ToM, a new link with a built-in interface for the F/T sensor was fabricated to replace the last link (i.e., the link closest to the stylus) of the PHANToM (see Fig. 5.1). The new link was of the same length as the original one, but weighed 60 g (13%) more. Force data were transformed into the stylus coordinate frame. The origin of the stylus coordinate frame was always located at the tip of the stylus (i.e., $\mathbf{p}(t)$), and its z-axis coincides with the cylindrical axis of the stylus (see Fig. 3.2).

Acceleration of the stylus was captured with a triaxial accelerometer (Kistler, Blairsville, PA; model 8794A500). The accelerometer was attached through a rigid mounter that was press-fitted to the stylus. The attachment added 11.8 g to the weight of the stylus. Acceleration measurements, $\mathbf{a}(t)$, were also taken in the stylus coordinate frame.

The effects of the sensor attachments on the device performance were investigated in terms of apparent inertia at the PHANToM stylus. We measured the tip inertia of the original and instrumented PHANToM devices along paths that passed the origin of the PHANToM coordinate frame. Two paths were chosen to be parallel to one of the axes of the PHANToM coordinate frame, differing in the direction of tip movement during

Table 5.1
Comparison of apparent tip inertia of the original and instrumented PHANToM devices.

Tip Movement Direction	Original PHANToM Tip Inertia (g)	Instrumented PHANToM Tip Inertia (g)	Effect of Sensor Attachment
$+x$	222.6	208.8	13.8 g decrease
$-x$	245.4	224.0	21.4 g decrease
$+y$	236.0	278.8	42.8 g increase
$-y$	282.4	143.0	139.4 g decrease
$+z$	97.2	126.6	29.4 g increase
$-z$	114.8	101.0	13.8 g decrease

the measurements (a total of six paths). The results are summarized in Table 5.1. It turned out that the tip inertia along the y-axis was affected most significantly by the the addition of the two sensors. In particular, the apparent tip inertia in the $-y$ direction (the direction of gravity) was reduced by 139.4 g. This was due to the fact that the additional sensor weight increased the effect of gravity on the corresponding tip inertia. The inertia along other directions changed in the range 13.8 g – 29.4 g, and were therefore much less affected by the additional sensor weight. Since the forces used in our experiments for rendering textured surfaces were confined in the x-z plane, we concluded, based on these measurements, that the instrumented PHANToM was able to reproduce the stimuli that led to perceived instability during the psychophysical experiments conducted earlier.

5.1.2 Subjects

Two subjects participated in the measurement experiment (one male, S1, and one female, S4). Their average age was 33 years old. Both are right-handed and report no

Table 5.2
Experimental conditions for measurement experiment using $d_1(t)$.

Exploration Mode	Texture Rendering Method	Perceptual Category	Texture Model Parameters A (mm), L (mm), K (N/mm)
Free Exploration	$\mathbf{F}_{mag}(t)$	Entry Instability	$1, 2, 0.30$
Free Exploration	$\mathbf{F}_{vec}(t)$	Entry Instability	$1, 2, 0.30$
Free Exploration	$\mathbf{F}_{vec}(t)$	Inside Instability	$1, 2, 0.05$
Stroking	$\mathbf{F}_{mag}(t)$	Stable	$1, 2, 0.15$
Stroking	$\mathbf{F}_{mag}(t)$	Unstable	$1, 2, 0.40$
Stroking	$\mathbf{F}_{vec}(t)$	Stable	$1, 2, 0.15$
Stroking	$\mathbf{F}_{vec}(t)$	Unstable	$1, 2, 0.40$

known sensory or motor abnormalities with their upper extremities. Only S1 had participated in the previous psychophysical experiments.

Both subjects were experienced users of the PHANToM device. They were preferred over naive subjects because the subjects had to place or move the stylus in a particular manner in order to maintain well-controlled conditions during data collection.

5.1.3 Experimental conditions

A total of seven experimental conditions was employed (see Table 5.2). In the conditions using free exploration, we collected data for the two primary instability categories of entry and inside instability. Note that inside instability with $\mathbf{F}_{mag}(t)$ was not tested because this type of instability had not been observed during our previous psychophysical experiments. For stroking, we recorded data under both stable and unstable conditions. Both texture rendering methods were tested for the stroking mode.

Whether a particular experimental condition resulted in the perception of instability depended on the values of the rendering parameters (A, L, and K). The values listed in Table 5.2 were selected based on the results obtained from our previous psychophysical experiments (see Fig. 4.3). We chose stiffness values that were either one standard deviation below the measured stiffness thresholds (for stable conditions) or one standard deviation above the thresholds (for unstable conditions).

5.1.4 Procedures

For the experiments with free exploration mode, the subjects were instructed to hold the stylus still near the textured surface (entry instability) or deep inside the textured surface (inside instability). They had to find a point in space where the surface was clearly perceived to be unstable and maintain that position. Once the subject was satisfied with the selected stylus position, the experimenter initiated data collection.

For the experiments with stroking mode, the subjects were instructed to move the stylus laterally across the virtual gratings. They were required to maintain a constant stroking speed to the best of their ability. After the subject had initiated stroking, the experimenter started data collection.

In all experimental conditions, the subjects were asked to hold the stylus like a pen (see Fig. 5.1). During each trial, three-dimensional position, force and acceleration data were collected for ten seconds at a sampling rate of 1 kHz.

5.1.5 Data analysis

Each ten-second long time-domain signal was processed as follows. Ten spectral densities corresponding to the ten one-second segments of the signal were computed and averaged for noise reduction. We used a flat-top window for the precise recovery of the magnitude of each spectral component [67]. The frequency and magnitude of each prominent spectral component in its corresponding physical units were then calculated.

In order to assess the perceived intensities of these spectral peaks, we compared their intensities in physical units to published human detection thresholds for sinusoidal movements. The human detection thresholds for vibrotactile stimuli depend on many factors including body site and contact area [68]. In our experiments, the stylus was in contact with the distal pads of three fingers (thumb, index finger, and middle finger), and the web between the thumb and the index finger. We therefore compared our measurements to the detection thresholds taken at the distal pad of the middle finger [69] and at the thenar eminence [70]. For both sets of data, we chose the threshold data taken with contactor areas that are closest to our experimental setup (0.3 cm^2 for finger tip and 1.3 cm^2 for thenar eminence). It turned out that the threshold curves from these two body sites are quite similar at their respectively chosen contact areas. We therefore used the detection thresholds for the thenar eminence at 1.3 cm^2 [70] for our data analysis. The perceived magnitude of a given spectral peak from the recorded signals was computed as the difference between the log of its intensity and the log of the human detection threshold at the same frequency. As is the common practice in psychophysics literature, these perceived magnitudes are expressed in dB SL (sensation level).

For stroking mode, we estimated the location of the spectral peak corresponding to texture information as follows. Suppose that a subject explored the textured wall by moving the stylus along the x-axis (see Fig. 3.3) with a constant velocity of v_x, while maintaining contact with the textured surface. Then, the magnitude of the rendered force could be decomposed into two terms. From Eqns. 3.3 and 3.4,

$$\left|\mathbf{F}_{mag}(t)\right| = \left|\mathbf{F}_{vec}(t)\right| = \left|KA\sin\left(2\pi\frac{v_x}{L}t\right) + K\left(A - p_z(t)\right)\right|, \tag{5.1}$$

assuming that $p_x(0) = 0$. The left term delivered the texture signal at frequency v_x/L, and the right term prevented the penetration of the stylus into the textured surface. Therefore, $\hat{f}_{tex}$, the estimated frequency for the spectral component responsible for texture perception, was

$$\hat{f}_{tex} = \frac{\overline{|v_x|}}{L}, \tag{5.2}$$

where $\overline{|v_x|}$ was the average stroking velocity.

5.2 Results

As an example of the collected data, the experimental results for stable stroking using $\mathbf{F}_{mag}(t)$ are shown in Fig. 5.2 for subject S4. Fig. 5.2(a), 5.2(b) and 5.2(c) represent the position, force, and acceleration measurements, respectively. In each figure, the measured 3D time-domain data are plotted in the upper panel, and the corresponding power spectral densities are shown in the lower panel. Note that the power spectral densities below 10 Hz are not shown because they are likely to be 1/f noises[2]. The predicted location ($\hat{f}_{tex}$) of the spectral component for texture information computed using Eqn. 5.2 was 50 Hz for this data set. As expected, all spectral densities in Fig. 5.2 showed spectral peaks around 50-60 Hz. We therefore infer that the mechanical energy in this frequency band was indeed responsible for the perception of desired virtual texture. It was also observed that no prominent peaks appear at higher frequencies for this condition. Furthermore, the locations of the distinct peaks measured with all three sensors were highly consistent, except for the high-frequency noise in the accelerometer data caused by quantization error. This consistency across sensor measurements turned out to be true for all experimental conditions. We therefore report only results obtained from the position data $p_z(t)$ in the remainder of this section. Note that $p_z(t)$ showed the largest power spectral density among the three positional variables, due to the fact that the normal vector of the underlying flat wall was in the z-direction (see Fig. 3.3).

For the free exploration conditions where all renderings were perceived to be unstable, the power spectral densities of $p_z(t)$ exhibited prominent spectral peaks in the frequency range 192-240 Hz. An example of such data (inside instability, $\mathbf{F}_{vec}(t)$, subject S1) is shown in Fig. 5.3(a). The upper panel contains the spectral density function (solid line) along with the detection thresholds taken from [70] (filled triangles) and the linearly-interpolated threshold curve (dotted line). The lower panel shows the difference between the power spectral density and the detection threshold curve. The dotted line indicates the reference line for 0 dB SL. In both panels, a vertical solid line is drawn to locate the

[2] 1/f noise refers to a noise that starts at 0 Hz and rapidly decays as frequency increases. This noise is very commonly observed in measured data [67].

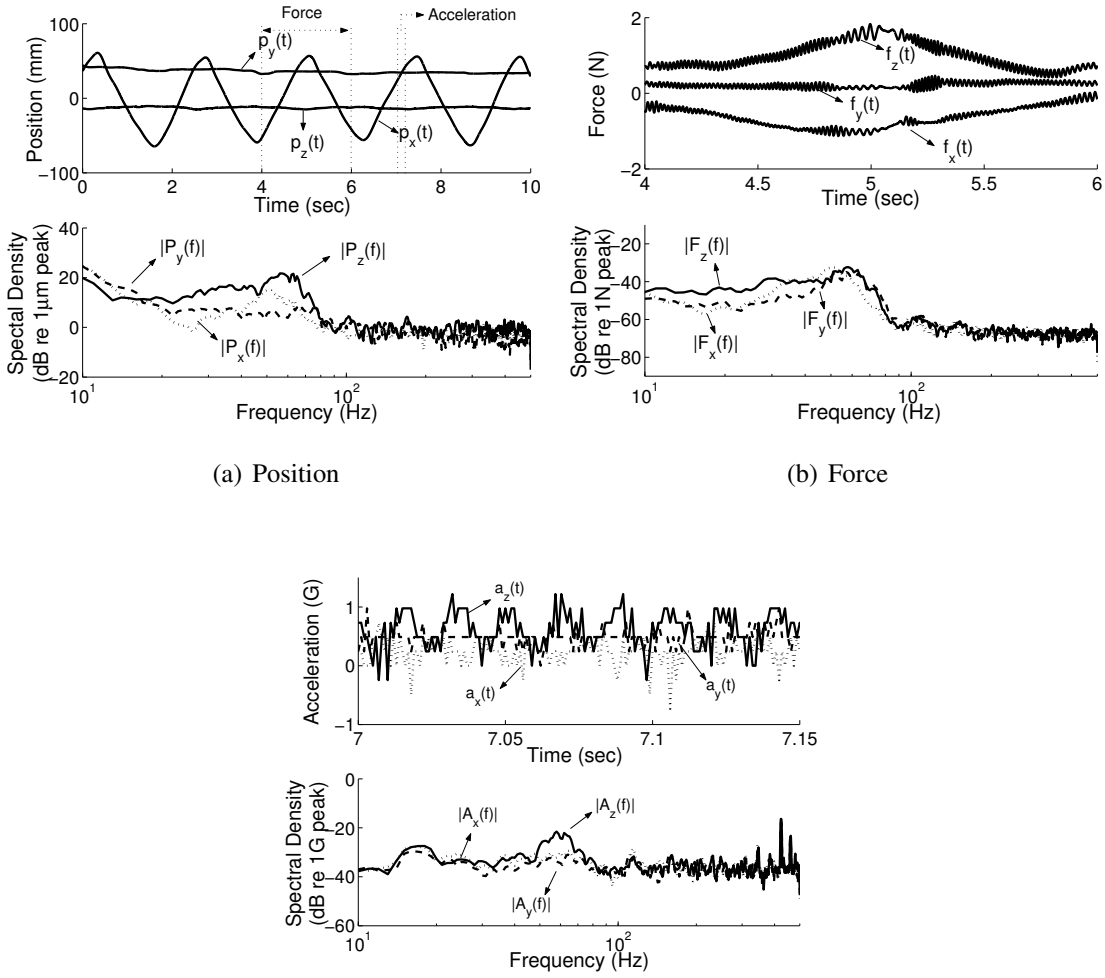

(a) Position

(b) Force

(c) Acceleration

Fig. 5.2. Experimental data for stable stroking (fixed-direction texture rendering method and subject S4). The measured time-domain data are shown in the upper panels, and their power spectral densities in the lower panels. The corresponding segments of Fig. 5.2(b) (force) and 5.2(c) (acceleration) are indicated in Fig. 5.2(a) (position).

Table 5.3
Predicted and measured locations of the spectral peaks for texture perception.

Condition	Subject	$\hat{f}_{tex}$ (Hz)	f_{tex} (Hz)
Stable stroking,	S1	40	51
$\mathbf{F}_{mag}(t)$	S4	50	56
Unstable stroking,	S1	29	26
$\mathbf{F}_{mag}(t)$	S4	39	41
Stable stroking,	S1	37	40
$\mathbf{F}_{vec}(t)$	S4	57	62
Unstable stroking,	S1	21	26
$\mathbf{F}_{vec}(t)$	S4	56	65

peak in the spectral density function. We observe that only the signal components around the spectral peak are significantly above the corresponding absolute detection thresholds. This fact was common to all experimental data for free exploration. It follows that the energy in this high-frequency band (denoted by f_{ins}) was responsible for the perception of instability.

For the stroking data, the predicted frequency $\hat{f}_{tex}$ for texture perception (see Eqn. 5.2) was used to locate its corresponding actual spectral peak (f_{tex}) in the recorded data. The results in Table 5.3 show a close agreement between the values of $\hat{f}_{tex}$ and f_{tex}, with an average prediction error of 5.5 Hz. Recall that $\hat{f}_{tex}$ was estimated under the assumption that the subject moved the stylus with a constant stroking velocity. This may have been the main source of discrepancy between the predicted and measured values of f_{tex}.

In the data measured under the conditions for perceptually stable stroking, only one spectral component that delivered texture information appeared in the power spectral densities. An example is shown in Fig. 5.3(b) ($\mathbf{F}_{mag}(t)$, subject S4). Note that only one spectral peak at 56 Hz (i.e., texture information) appears in this figure.

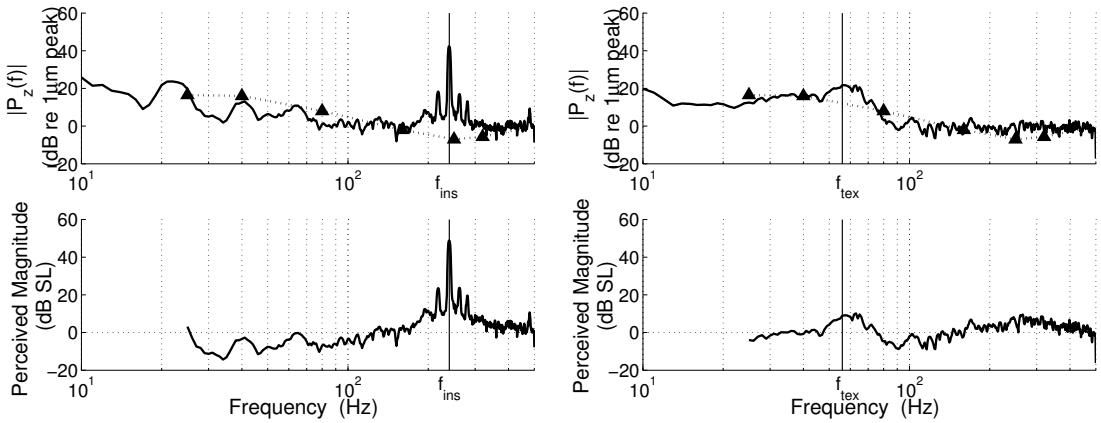

(a) Inside instability, $\mathbf{F}_{vec}(t)$, subject S1

(b) Stable stroking, $\mathbf{F}_{mag}(t)$, subject S4

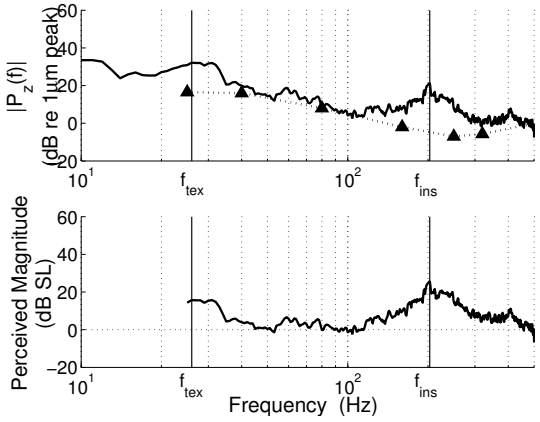

(c) Unstable stroking, $\mathbf{F}_{mag}(t)$, subject S1

Fig. 5.3. Average power spectral density of $p_z(t)$ and their corresponding sensation levels. The upper panels show the spectral densities (solid lines) with the detection thresholds at the thenar eminence (triangles and dashed lines). The lower panels show the sensation levels as the difference between spectral densities and detection thresholds. The vertical lines mark the spectral components for texture perception (f_{tex}) and for perceived instability (f_{ins}).

For the conditions under which the subjects felt instability during stroking, usually two distinctive spectral components were observed in the measured power spectral densities of $p_z(t)$. Fig. 5.3(c) shows an example ($\mathbf{F}_{mag}(t)$, subject S1) of such cases . This spectral density function shows two prominent peaks at $f_{tex} = 26$ Hz (texture information) and $f_{ins} = 203$ Hz (perception of instability).

Finally, the perceived magnitudes of spectral components at f_{tex} and f_{ins} are summarized in Table 5.4 for every experimental condition and every subject. The average values of f_{tex} and f_{ins} were 45.9 and 213.7 Hz, respectively. The range of f_{tex} (26-65 Hz) was well separated from that of f_{ins} (192-240 Hz). Perceived magnitudes ranged from 4.95 to 23.61 dB SL for f_{tex} components and 21.21 to 48.79 dB SL for f_{ins} components, respectively.

5.3 Discussion

In these experiments, we measured position, force and acceleration signals experienced by the human hand during exploration of virtual textures. Data were recorded for free exploration and stroking modes using two rendering methods under both stable and unstable rendering conditions. As we stated earlier, our first goal was to isolate signal components responsible for the perception of instability. From our psychophysical experiments conducted earlier, we learned that subjects relied on the detection of a "buzzing" vibration to declare a virtual textured surface to be unstable. This indicated a signal with spectral components above 100 Hz [71]. Indeed, we were able to isolate signal components in the frequency range of 192–240 Hz from the measurements taken during unstable texture rendering conditions. This happens to be the frequency range at which humans are most sensitive to vibrational stimulation [68]. From the measurement experiments, we were also able to predict, then locate the spectral components responsible for texture information in the frequency range of 26–65 Hz. Stimulation in this frequency range is usually perceived to be "rough" and "fluttering" [72] [71]. In order to characterize the perceptual intensities of measured signals, the magnitudes of their spectral peaks were converted to

Table 5.4
Intensities of spectral peaks (in sensation level) at frequencies for texture perception (f_{tex}) and instability perception (f_{ins}).

Condition	Subject	SL (dB) @ f_{tex} (Hz)	SL (dB) @ f_{ins} (Hz)
Entry instability,	S1	—	39.31 @ 223
$\mathbf{F}_{mag}(t)$	S4	—	33.48 @ 221
Entry instability,	S1	—	47.84 @ 238
$\mathbf{F}_{vec}(t)$	S4	—	33.01 @ 192
Inside instability,	S1	—	48.79 @ 240
$\mathbf{F}_{vec}(t)$	S4	—	30.92 @ 205
Stable stroking,	S1	4.95 @ 51	—
$\mathbf{F}_{mag}(t)$	S4	8.91 @ 56	—
Unstable stroking,	S1	15.67 @ 26	25.89 @ 203
$\mathbf{F}_{mag}(t)$	S4	10.98 @ 41	25.57 @ 194
Stable stroking,	S1	8.28 @ 40	—
$\mathbf{F}_{vec}(t)$	S4	13.83 @ 62	—
Unstable stroking,	S1	8.73 @ 26	21.21 @ 208
$\mathbf{F}_{vec}(t)$	S4	23.61 @ 65	26.53 @ 203

perceived magnitudes in dB SL. While the intensities of the signals conveying texture information were of intermediate magnitude (4.95–23.61 dB SL), the high-frequency noises that gave rise to the perception of instability were generally "louder" (21.21–48.79 dB SL) in terms of perception.[3]

The frequency ranges for texture and instability perception are not only well separated in their numerical values, but in the neural mechanism mediating their perception as well. From an engineering point of view, one of the most important performance criteria for any stabilization technique for haptic rendering is the minimization of the loss of perceptual information due to stabilization [32]. The fact that the two frequency ranges responsible for texture and instability perception are numerically well separated suggests that it ought to be possible to filter out the high-frequency spectral components responsible for instability perception without significantly altering the signals containing texture information. From a perception point of view, it is well established in haptic perception literature that two mechanoreceptive afferents types, the slowly adapting type 1 and the Pacinian system, are responsible for the perception of signals in the 26–65 Hz and the 192–240 Hz frequency ranges, respectively [68] [74]. When signals in these two frequency regions are combined, they remain perceptually salient and distinctive. Therefore, our subjects were able to simultaneously perceive the spectral peaks responsible for texture and instability.

In an attempt to locate the sources of the high-frequency signals responsible for perceived instability, we measured a z-axis open-loop frequency response of the PHANToM with the tip of the stylus resting at the origin of its world coordinate frame. During the measurement, the stylus was supported by a tight string anchored from above which served to constrain the stylus to point towards the $+z$-direction. The stylus of the PHANToM could only move along the z-axis. This frequency response is defined as

$$|H_z(f)| = \left| \frac{P_z(f)}{\widetilde{F_z}(f)} \right|, \tag{5.3}$$

[3] According to [73], stimulation levels exceeding 50-55 dB SL start to induce discomfort and fatigue.

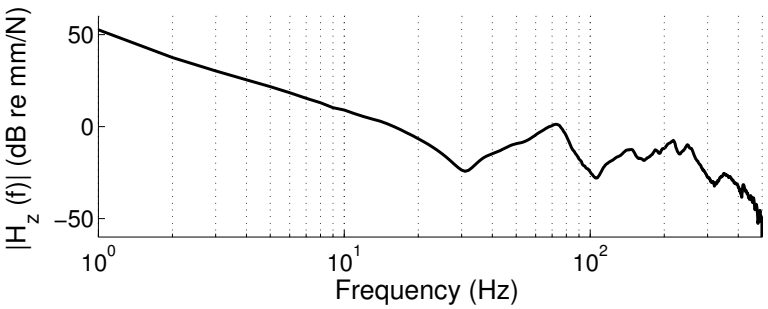

Fig. 5.4. Frequency response of the PHANToM (model 1.0A) measured at the origin and along the z-axis of its world coordinate frame.

where $\widetilde{F}_z(f)$ is the Fourier transform of the z-axis force command to the PHANToM, and $P_z(f)$ is that of the z-axis position of the stylus tip. The result, shown in Fig. 5.4, indicates a mechanical resonance at 218 Hz. A similar resonance frequency has also been reported recently for model 1.5 of the PHANToM [75]. This resonance is well within the 192–240 Hz frequency range. Therefore, it seems to be the source of the spectral peaks in the frequency range that we had identified to be responsible for instability perception. Since humans are most sensitive to vibrations within this frequency range, noise produced by this resonance tends to be "loud" perceptually.

6. QUANTIFICATION OF PERCEIVED INSTABILITY: PART II

[1]This chapter presents the experimental design and results of the second part of our psychophysical experiments. These experiments used $d_2(t)$ in Eqn. 3.2 for the computation of penetration depths. The experimental design was essentially the same as that of the first part of our experiments discussed in Ch. 4.

As mentioned earlier, the new collision detection algorithm based on $d_2(t)$ eliminated the step changes in force magnitudes suffered by the method based on $d_1(t)$. We therefore expected the perceived quality of virtual haptic textures to improve with the new algorithm. The experiments reported in this chapter were conducted to asses the extent of the expected improvement.

6.1 Experiment Design

6.1.1 Apparatus

A PHANToM force-reflecting haptic interface (model 1.0A with a stylus and an encoder gimbal) was used in all experiments to render virtual textured surfaces.

6.1.2 Subjects

Three subjects (one male, S1, and two females, S2 and S4) participated in the experiments. S1 and S2 also participated in our previous experiments. S1 and S4 are experienced users of the PHANToM device. S2 had not used any haptic interface prior to her participation in the psychophysical experiments reported in Ch. 5. The average age

[1]The materials presented in Chs. 6 and 7 have been submitted to *Presence: Teleoperators and Virtual Environments* in S. Choi and H. Z. Tan, "Perceived Instability of Virtual Haptic Texture. II. Effect of Collision Detection Algorithm."

of the subjects was 33.6 years old. All subjects are right-handed and reported no known sensory or motor abnormalities with their upper extremities.

6.1.3 Stimuli

The virtual textured surfaces were modeled as one-dimensional sinusoidal gratings with amplitude A and spatial wavelength L, superimposed on a flat surface (see Fig. 3.3).

Two texture rendering methods, one based on [44] (denoted by $\mathbf{F}_{mag}(t)$) and the other on [39] (denoted by $\mathbf{F}_{vec}(t)$), were employed. The two methods produced the same force magnitude of $K \cdot d_2(t)$, where K was the surface stiffness and $d_2(t)$ was the penetration depth as defined in Eq. 3.2. The $\mathbf{F}_{mag}(t)$ method rendered a force with a constant direction that was normal to the underlying flat wall ($\mathbf{n}_W$ in Fig. 3.3). The $\mathbf{F}_{vec}(t)$ method rendered a force in a direction that stayed normal to the sinusoidal textured surface ($\mathbf{n}_T(\mathbf{p}(t))$ in Fig. 3.3). The main difference between the stimuli used in the present study and those reported in Ch. 4 was the way with which penetration depth was calculated. While the previous study used $d_1(t)$ in Eq. 3.1 for penetration depth computation, the current study employed $d_2(t)$ in Eq. 3.2.

The stimuli used in the current study were uniquely defined by the amplitude (A) and wavelength (L) of the sinusoidal texture model, the surface stiffness (K), and the texture rendering method.

6.1.4 Experimental conditions

Two exploration modes, free exploration and stroking, were tested in order to examine the effect of an user interaction pattern on perceived instability. In the free exploration mode, subjects were allowed to use the interaction pattern that they found most effective at discovering instability of virtual textures. In the stroking mode, subjects were instructed to move the stylus laterally across the textured surface.

Four experiments were defined by the combinations of the two texture rendering methods and the two exploration modes (see Table 6.1). Five combinations of A and L

Table 6.1
Experimental conditions of psychophysical experiments using $d_2(t)$.

Experiment	Texture Rendering Method	Exploration Mode	Texture Model Parameters (A (mm), L (mm))
II-1	$\mathbf{F}_{mag}(t)$	Free Exploration	(0.5, 2.0), (1.0, 1.0), (1.0, 2.0), (1.0, 4.0), (2.0, 2.0)
II-2	$\mathbf{F}_{mag}(t)$	Stroking	(0.5, 2.0), (1.0, 1.0), (1.0, 2.0), (1.0, 4.0), (2.0, 2.0)
II-3	$\mathbf{F}_{vec}(t)$	Free Exploration	(0.5, 2.0), (1.0, 1.0), (1.0, 2.0), (1.0, 4.0), (2.0, 2.0)
II-4	$\mathbf{F}_{vec}(t)$	Stroking	(0.5, 2.0), (1.0, 1.0), (1.0, 2.0), (1.0, 4.0), (2.0, 2.0)

were used per experiment. They were a subset of the conditions tested in the previous study reported in Ch. 4. The dependent variable measured was the maximum stiffness below which the rendered textured surface was perceived to be stable.

6.1.5 Procedure

The experimental procedure was essentially the same as that employed in Ch. 4. The method of limits was used to estimate the maximum stiffness threshold under which the virtual haptic textures were perceived to be stable. Based on preliminary results, the maximum stiffness (K_{max}) was set to 1.0 N/mm and 1.6 N/mm for free exploration (Exps. II-1 and II-3) and stroking (Exps. II-2 and II-4), respectively. The stiffness increment ΔK was fixed at 0.05 N/mm for all conditions. The order of the four experiments as well as that of the five experimental conditions within each experiment was randomized for each subject.

6.2 Results

Stiffness thresholds (denoted by K_T) under which the textured surfaces were perceived to be stable are shown in Fig. 6.1 for the four experiments. In each plot, the average K_T values are represented by circles. The error bars represent ± 1 standard deviations. Dashed lines are used to project the symbols to the A-L plane. The mean stiffness thresholds ranged 0.1707–0.5497 N/mm, 0.2490–0.7097 N/mm, 0.0204–0.0256 N/mm, and 0.3877–0.7786 N/mm for Exps. II-1, II-2, II-3, and II-4, respectively. A five-way ANOVA performed on the data pooled from all subjects showed that all five factors of A, L, texture rendering method, exploration mode, and subject had a significant effect on the K_T values ($F(2,5940) = 427.83$, $F(2,5940) = 1703.39$, $F(1,5940) = 1891.89$, $F(1,5940) = 10396.2$, and $F(2,5940) = 3551.86$, respectively; $p < 0.0001$ for all factors; $R^2 = 0.89$).

A general trend in Fig. 6.1 is that K_T increased with wavelength (L) and decreased with amplitude (A), except for the mean thresholds in Exp. II-3 that were too small to exhibit any trend. To investigate this trend, we performed a three-way ANOVA analysis with the three factors of A, L, and subject on the pooled data for Exps. II-1, II-2 and II-4. Due to the fact that subject was a significant factor, we also ran a two-way ANOVA analysis with the two factors of A and L on individual data. These statistical analyses showed that in Exps. II-1 and II-4, both A and L were significant factors on individual as well as pooled data ($p < 0.0001$ for each combination of factor and experiment). In Exp. II-2, A was a significant factor for both pooled and individual data ($F(2,1485) = 1215.23$ with $p < 0.0001$ for the pooled data; $p < 0.0001$ for each individual data set). However, the effect of L depended on individual subjects. L was not a significant factor for the data of subjects S1 or S4 ($F(2,495) = 0.44$ with $p = 0.6424$ and $F(2,495) = 1.40$ with $p = 0.2468$, respectively), but was a significant factor for subject S2's data ($F(2,495) = 839.75$ with $p < 0.0001$). L was also a significant factor in the pooled data ($F(2,1485) = 6.15$ with $p < 0.0022$). Thus, we conclude that in Exp. II-2 the effect of L on K_T values

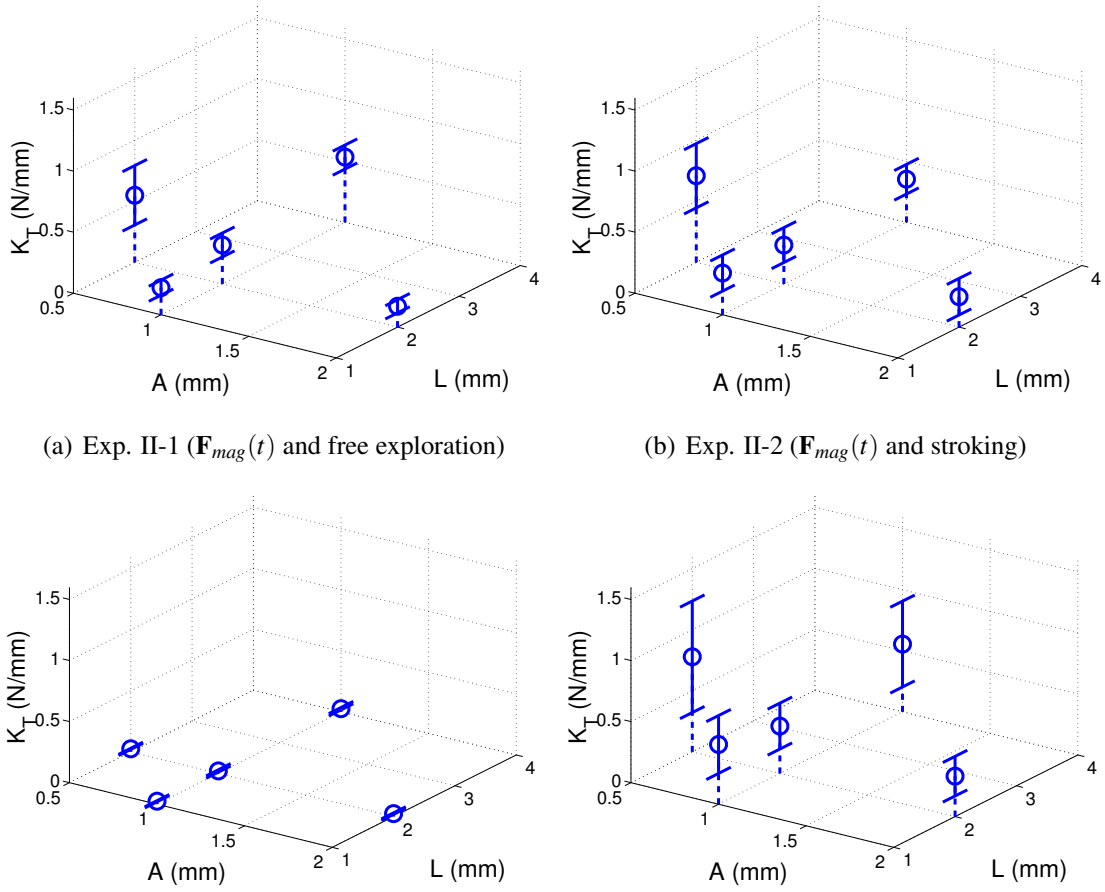

(a) Exp. II-1 ($\mathbf{F}_{mag}(t)$ and free exploration)

(b) Exp. II-2 ($\mathbf{F}_{mag}(t)$ and stroking)

(c) Exp. II-3 ($\mathbf{F}_{vec}(t)$ and free exploration)

(d) Exp. II-4 ($\mathbf{F}_{vec}(t)$ and stroking)

Fig. 6.1. Results of psychophysical experiments using $d_2(t)$.

($p = 0.0022$ in the pooled data) was weaker than that of A ($p < 0.0001$ in the pooled data).

In terms of texture rendering method, the textured surfaces rendered with $\mathbf{F}_{mag}(t)$ resulted in significantly larger stiffness thresholds than those with $\mathbf{F}_{vec}(t)$ for the free exploration mode (mean difference = 0.3353, $t = 159.10$, $p < 0.0001$). For the stroking mode, the reverse was true (mean difference = -0.1138, $t = 24.52$, $p < 0.0001$): larger stiffness thresholds were obtained with $\mathbf{F}_{vec}(t)$. This was mainly due to the relatively large differences in subject S4's data in Exps. II-2 and II-4 that exhibited a trend opposite to that observed with subjects S1 and S2. In terms of exploration mode, stroking resulted in higher stiffness thresholds than free exploration (mean difference = 0.2597, $t = 101.96$, $p < 0.0001$ in the pooled data). Statistical analyses performed on individual subject's data confirmed the effect of exploration mode that was observed in the pooled data ($p < 0.0001$ in each individual data set).

6.3 Discussion

In the psychophysical experiments, we measured the maximum stiffness values under which a virtual textured surface rendered with a force-feedback device was perceptually "clean" and stable. The collision detection algorithm employed in this study was based on the relative position of the stylus tip and the height of the sinusoidal surface texture (Eq. 3.2). The experimental conditions used in these experiments were a subset of those used in our previous study reported in Ch. 4 in which we employed a collision detection algorithm based on the relative position of the stylus tip and the flat wall underlying the textured surface (Eq. 3.1). We can examine the effect of collision detection algorithms on the perceived quality of virtual haptic textures by comparing the results from our previous and current experiments.

Table 6.2 presents the ranges and means of stiffness thresholds K_T from the current study and from the previous study for each experiment. Only the data from subjects S1 and S2 who participated in both studies were used for the comparison. We found that switching

Table 6.2
Comparison of stiffness thresholds measured in the current and previous experiments. All stiffness values are in N/mm. Only data of subjects S1 and S2 are shown.

Experiments	Experiments II ($d_2(t)$)		Experiment I ($d_1(t)$)	
	Range	Mean	Range	Mean
1. $\mathbf{F}_{mag}(t)$, free exploration	0.1813 – 0.5383	0.3486	0.0586 – 0.1023	0.0799
2. $\mathbf{F}_{mag}(t)$, stroking	0.2490 – 0.6410	0.3603	0.4488 – 0.1664	0.3116
3. $\mathbf{F}_{vec}(t)$, free exploration	0.0181 – 0.0260	0.0235	0.0097 – 0.0367	0.0209
4. $\mathbf{F}_{vec}(t)$, stroking	0.3254 – 0.4638	0.3808	0.0718 – 0.3292	0.1848

from $d_1(t)$ to $d_2(t)$ resulted in a statistically significant increase in the stiffness thresholds obtained in Exps. II-1, II-2, and II-4 (average difference = 0.2687 N/mm, 0.0487 N/mm and 0.1960 N/mm, respectively; $t = 62.68$, 7.44, and 40.07, respectively; $p < 0.0001$ for all experiments), but not those in Exp. II-3 (average difference = 0.0026 N/mm, $t = 1.17$, $p = 0.2403$). Numerically, however, only the threshold increases in Exps. II-2 and II-4 were substantial.

The observed effects of collision detection algorithms on perceived instability were consistent with our initial expectations for data obtained in Exps. II-1 and II-3, but not for those obtained in Exps. II-2 and II-4. In Exps. II-1 ($\mathbf{F}_{mag}(t)$, free exploration) and II-3 ($\mathbf{F}_{vec}(t)$, free exploration), the subjects were allowed to explore the virtual haptic textures freely, including moving the PHANToM stylus in and out of the virtual surfaces. Recall that the main difference between the collision detection algorithms used in the current and previous experiments was that the new algorithm rendered forces that were continuous at the boundary of the virtual textured surfaces. We therefore expected higher stiffness thresholds in the current study. The results from Exp. II-1 confirmed our expectation. The stiffness thresholds obtained in Exp. II-3, however, were uniformly low (i.e., below the step size of 0.05 N/mm used in the method of limits). The subjects reported that they felt

high-frequency "buzzing" noises whenever the stylus was positioned inside the textured surfaces. The same was also frequently observed in our previous study reported in Ch. 4. This fact indicates that the rapid changes in force directions due to $\mathbf{F}_{vec}(t)$ significantly decreased the perceived stability of virtual textures to the extent that any improvement in stability due to the new collision detection algorithm could not be observed.[2] In Exps. II-2 ($\mathbf{F}_{mag}(t)$, stroking) and II-4 ($\mathbf{F}_{vec}(t)$, stroking), the subjects were instructed to move the PHANToM stylus laterally across the virtual haptic textures. Assuming that the subjects kept the stylus inside the textured surface during stroking, we did not expect to observe any significant changes in stiffness thresholds with the new collision detection algorithm. The results from Exps. II-2 and II-4 demonstrated a statistically significant increase in the mean stiffness threshold. To seek an explanation for this unexpected result, we examined the position data measured from these two experiments, and report our findings in Sec. 7.4.

The types of sensations associated with perceived instability were unveiled through subject debriefing. The sensations seemed to depend more on how the forces were rendered than on exploration mode. In Exps. II-1 and II-2 (both using $\mathbf{F}_{mag}(t)$)), when the stiffness values were well above the measured thresholds, the subjects felt high-frequency "buzzing" noises and used that sensation to declare unstable textures. The same phenomenon was also frequently observed in our previous experiments. When the values of surface stiffness were lowered to be slightly above the measured thresholds, however, the subjects often reported that the textured surfaces appeared to be "alive." Very often, the subject felt force perturbations that could not be attributed to any movements that they had initiated. This type of perceived instability was not discovered in our previous study. The sensations associated with perceived instability in Exps. II-3 and II-4 (both using $\mathbf{F}_{vec}(t)$) were very similar to those reported in our previous study. The major two types of sensations were buzzing and "ridge instability". The latter describes the phenomenon where

[2]The authors of the $\mathbf{F}_{vec}(t)$ rendering method [39] were aware of the instability problem, and developed a heuristic algorithm that interpolated the direction of a force vector between the normal to the texture model (for small penetration depth) and that to the underlying surface (for large penetration depth). We were interested in investigating the generic performance of $\mathbf{F}_{vec}(t)$ and therefore did not incorporate the interpolation scheme in our experiments on perceived instability.

the net force exerted by the PHANToM on the stylus tip pointed towards a valley of the sinusoidal gratings when a subject attempted to rest the stylus on a ridge. More details can be found in Chs. 4 and 5.

The results of the psychophysical experiments showed that the choice of a collision detection algorithm clearly influenced the perceived stability/instability of virtual haptic textures. A new type of perceived instability, aliveness, was also discovered. In order to gain further insight into how the two types of perceived instability (buzzing and aliveness) depended on the collision detection algorithm and other factors, we measured the proximal stimuli at the PHANToM stylus under a variety of conditions and report the results in the next section.

7. CHARACTERIZATION OF PROXIMAL STIMULI: PART II

[1]In this chapter, we report the results of measurement experiments that identified the proximal stimuli responsible for perceived instability observed in the psychophysical experiment using $d_2(t)$. After presenting the methods used in the measurement experiments, we focus our discussion on the following issues.

- Was buzzing caused by high-frequency signals, as was the case in our previous study using the $d_1(t)$ collision-detection algorithm?
- What proximal stimuli were responsible for the perception of aliveness?
- Why did stiffness thresholds increase significantly in Exps. II-2 and II-4 although we did not expect them to?
- Was aliveness perception caused by device instability, as was the case with buzzing?

7.1 Experiment Design

The PHANToM force-reflecting device instrumented with two additional sensors (a force/torque sensor and an accelerometer) was used for haptic texture rendering and data collection (see Fig. 5.1). This instrumented PHANToM was capable of sensing three-dimensional (3-D) position, force, and acceleration of the stylus. See Sec. 4.1.1 for the details of the sensors used and the modifications made to the PHANToM.

Two subjects (S1 and S4) participated in the measurement experiment. Both subjects were experienced users of the PHANToM device. They were preferred over naive

[1]The materials presented in Chs. 6 and 7 have been submitted to *Presence: Teleoperators and Virtual Environments* in S. Choi and H. Z. Tan, "Perceived Instability of Virtual Haptic Texture. II. Effect of Collision Detection Algorithm."

subjects because they were required to place or move the stylus in a particular manner in order to maintain well-controlled conditions during data collection.

Experimental conditions used in the measurement experiment differed in texture rendering parameter (A and L), texture rendering method ($\mathbf{F}_{mag}(t)$ and $\mathbf{F}_{vec}(t)$), exploration mode (free exploration and stroking), and perceptual category (stable and unstable). The values of surface stiffness (K) were selected to result in either perceptually stable or unstable rendering based on the results of the psychophysical experiments.

For the experiments with free exploration mode, the subjects were instructed to hold the stylus stationary near or deep inside the textured surface. They had to find a point in space where the textured surface was clearly perceived to be unstable and maintain that position. Once the subject was satisfied with the selected stylus position, the experimenter initiated data collection. For the experiments with stroking mode, the subjects were instructed to move the stylus laterally across the virtual gratings. They were required to maintain a constant stroking speed to the best of their ability. After the subject had initiated stroking, the experimenter started data collection. In all experimental conditions, the subjects were asked to hold the stylus like a pen (see Fig. 5.1). During each trial, 3-D position, force and acceleration data were collected for ten seconds at a sampling rate of 1 kHz.

Each segment of ten-second long measured data was analyzed in both time and frequency domains. In the frequency-domain analysis of stroking condition, the location of the spectral peak corresponding to texture information was estimated by $\hat{f}_{tex} = \overline{|v_x|}/L$, where $\overline{|v_x|}$ was the average stroking velocity. The actual frequency (f_{tex}) was then determined from the location of the spectral peak closest to $\hat{f}_{tex}$ in the recorded data. The perceived magnitude of any spectral component was converted from its physical unit to "sensation level" by taking the difference between the log of its intensity and the log of the human detection threshold at the same frequency. See Sec. 5.1.5 for further details of data analysis.

7.2 Was Buzzing Caused by High-Frequency Signals?

Recall that buzzing often occurred when a high stiffness value was used in haptic texture rendering. In our measured data, we were able to observe a high-frequency spectral peak whenever buzzing was perceived. Fig. 7.1 provides an example of the high-frequency noise associated with the perception of buzzing for free exploration (panel (a)) and stroking (panel (b)). In both panels, the spectral densities for position signal $p_z(t)$ (perpendicular to the wall underlying the textured surface) are shown as solid lines, and the human detection thresholds are shown as dashed lines with triangles (reproduced from [70]). The data shown in Fig. 7.1(a) were taken with the stylus tip positioned near the textured surface ($\mathbf{F}_{mag}(t)$, free exploration, buzzing). We can observe several spectral peaks at a frequency of 169 Hz (marked f_{ins} for instability frequency) or higher. The intensity of the spectral peaks were as much as 7 dB above human detection thresholds indicating that they could be perceived by our subjects. We therefore conclude that these high-frequency spectral components contributed to the perception of buzzing.

Fig. 7.1(b) shows data recorded while the subject stroked the textured plane ($\mathbf{F}_{mag}(t)$, stroking, buzzing). We can observe one spectral peak at 71 Hz (marked f_{tex} for texture frequency) and several spectral peaks at 150 Hz (marked f_{ins}) and higher. The location of f_{tex} was consistent with that estimated from the spatial frequency L of the texture model and the measured stroking velocity. Therefore, this spectral component provided the temporal cues for the perception of the textured surface during stroking. The high-frequency spectral peaks were as much as 25 dB above human detection thresholds and therefore contributed to a strong sensation of buzzing.

Results obtained with textured surfaces rendered with $\mathbf{F}_{vec}(t)$ exhibited similar high-frequency spectral peaks whenever buzzing was perceived. Together, the measurement data obtained in the current study were consistent with those obtained in our previous study (see Ch. 5) in that high-frequency spectral peaks with intensities above human detection thresholds were responsible for the perception of buzzing that made virtual haptic

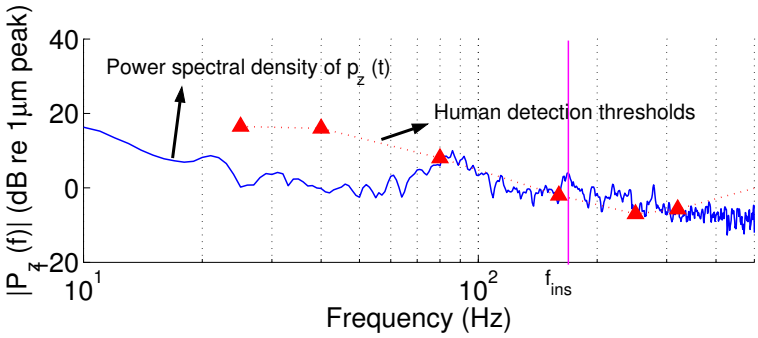

(a) Spectral density of position data measured with $\mathbf{F}_{mag}(t)$ and free exploration (A = 1.0 mm, L = 2.0 mm, and K = 1.0 N/mm).

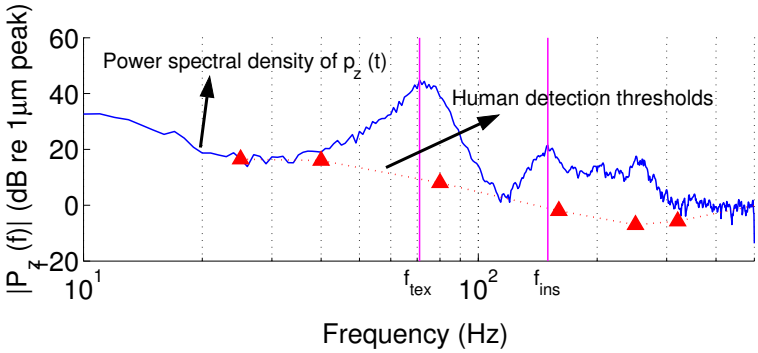

(b) Spectral density of position data measured with $\mathbf{F}_{mag}(t)$ and stroking (A = 1.0 mm, L = 2.0 mm, and K = 1.2 N/mm).

Fig. 7.1. Illustration of high-frequency noise associated with the "buzzing" type of perceived instability.

textures feel unstable. Therefore, the choice of a collision-detection algorithm did not change the underlying cause for the perception of buzzing.

7.3 What Signals were Responsible for Aliveness?

When the stiffness of the textured surface rendered using $\mathbf{F}_{mag}(t)$ was lowered to be slightly above the threshold for perceptually stable texture rendering, the subjects reported that the apparent aliveness of the surface became the dominant cue for perceived instability. Consistent with the subjects' observation, no prominent high-frequency spec-

tral peaks were observed in the power spectral densities of recorded data (measured with stiffness values one standard deviation above the thresholds). Instead, we found many instances where a relatively large force variation occurred while the PHANToM stylus barely moved along the direction of the force variation. Fig. 7.2 illustrates this finding with position and force data measured during free exploration (panel (a)) and stroking (panel (b)). In both panels, force variation along the cylindrical axis of the stylus, $F_z^S(t)$, is plotted against the displacement of the stylus in two directions, $p_x(t)$ (along the direction of stroking) and $p_z(t)$ (along the direction of surface-height variation), for a period of 400 ms. Also shown in both panels of Fig. 7.2 are the three projections of measured force. We did not plot $F_z^S(t)$ against $p_y(t)$ since our texture model did not vary along the y-axis.

The data shown in Fig. 7.2(a) were taken with the stylus tip held stationary near the textured surface ($\mathbf{F}_{mag}(t)$, free exploration, aliveness). The projection on the $p_x(t)$-$p_z(t)$ plane shows that the stylus tip moved by less than 0.56 mm in the x-direction and 0.94 mm in the z-direction. These movement magnitudes are barely perceivable when the hand is held in free space[2]. The corresponding change in force magnitude, however, was large enough to be clearly perceived ($\max F_z^S(t) - \min F_z^S(t) = 0.59$ N). Since the subject was under the impression that the PHANToM stylus was held still in space, the perceived force variation was attributed to an "alive" virtual textured surface rather than to the slight tremor of the subject's hand.

The same phenomenon can be observed in Fig. 7.2(b) with data collected during stroking ($\mathbf{F}_{mag}(t)$, stroking, aliveness). In this figure, the large change in $p_x(t)$ was the result of the subject's stroking movement. While the force data ($F_z^S(t)$) felt by the subject exhibited magnitude variations on the order of 0.5 N, the change in position along the direction of surface-height variation ($p_z(t)$) was hardly perceptible (less than 1 mm). As a result, the subject felt a noticeable force change through the stylus although the stylus was perceived to be barely moving in and out of the textured surface. It follows that this

[2]We were not able to find detection thresholds for hand movement in free space in the literature to compare these numbers against.

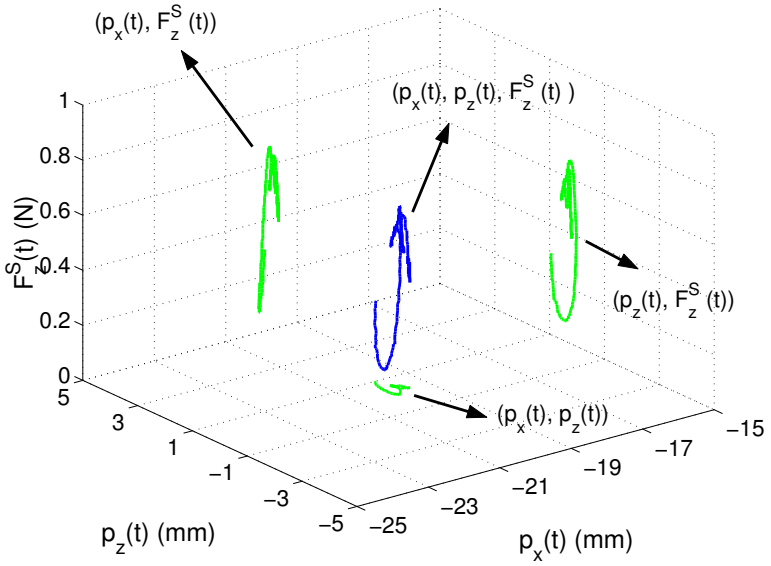

(a) Force and position data measured with $\mathbf{F}_{mag}(t)$ and free exploration (A = 1.0 mm, L = 1.0 mm, and K = 0.4 N/mm).

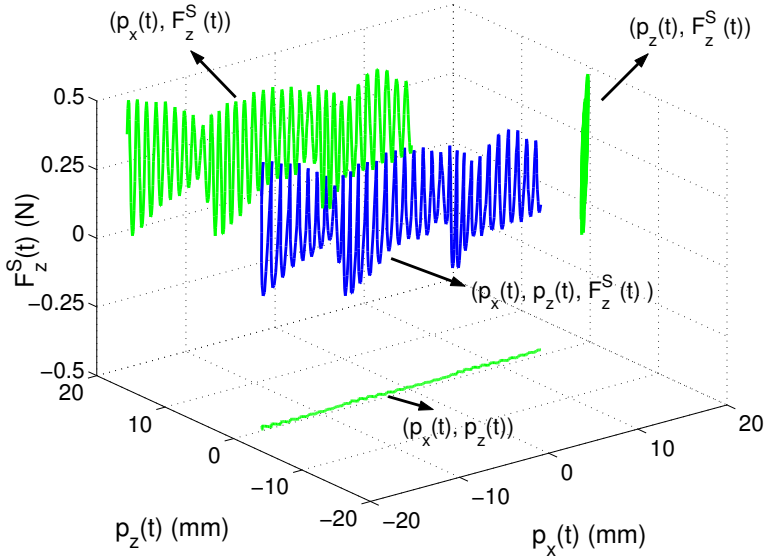

(b) Force and position data measured with $\mathbf{F}_{mag}(t)$ and stroking A = 1.0 mm, L = 1.0 mm, K = 0.5 N/mm).

Fig. 7.2. Characteristics of aliveness.

force variation was interpreted as coming from an "alive" textured surface. The subjects commented that they felt the surface "pulsating" during stroking.

7.4 Why did Stiffness Thresholds Increase in Exps. II-2 and II-4?

Recall that the main difference between the two collision detection algorithms $d_1(t)$ and $d_2(t)$ was that $d_1(t)$ introduced step changes at the entry points along the textured surface but $d_2(t)$ did not. Also recall that the two psychophysical experiments II-2 and II-4 employed stroking mode. To the extent that the PHANToM stylus remained underneath the textured surface during stroking, we did not expect to see a significant increase in stiffness thresholds in the current study using $d_2(t)$ as compared to those obtained in our earlier study using $d_1(t)$. However, it was found that stiffness thresholds increased significantly in both Exp. II-2 ($\mathbf{F}_{mag}(t)$, stroking) and Exp. II-4 ($\mathbf{F}_{vec}(t)$, stroking).

In order to explain this threshold increase, we examined the stylus positions recorded during these two experiments. Fig. 7.3 shows typical data traces for $p_x(t)$ (position along the stroking direction), $p_z(t)$ (position along the surface-height variation), and $d_2(t)$ (calculated penetration depth). Also shown with $p_z(t)$ (solid lines) are the height of the sinusoidal textured surface computed at $(p_x(t), p_z(t))$ (dotted lines), and the underlying wall (straight dashed lines). The duration of each data trace is 500 ms. It can be seen from the middle panel of Fig. 7.3(a), the PHANToM stylus did not remain inside the textured surface at all times. Instead, the stylus remained somewhere between the peaks and valleys of the sinusoidal height variations. The same can be observed from the middle panel of Fig. 7.3(b). Therefore, our assumption that the PHANToM stylus remained inside the textured surfaces during stroking was not valid. Furthermore, we observe from the bottom panels of both Fig. 7.3(a) and Fig. 7.3(b) that there were no abrupt step changes in the calculated penetration depths, and therefore no abrupt changes in force commands that were related to the penetration depths by a constant stiffness. These results explain why the stiffness thresholds obtained in Exps. II-2 and II-4 increased significantly in the current study.

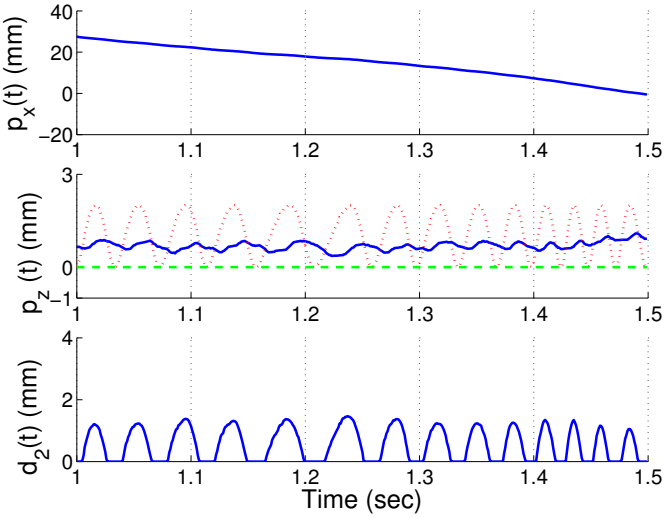

(a) Position data recorded from Exp. II-2 ($\mathbf{F}_{mag}(t)$, stroking, $d_2(t)$, and $K = 0.6$ N/mm).

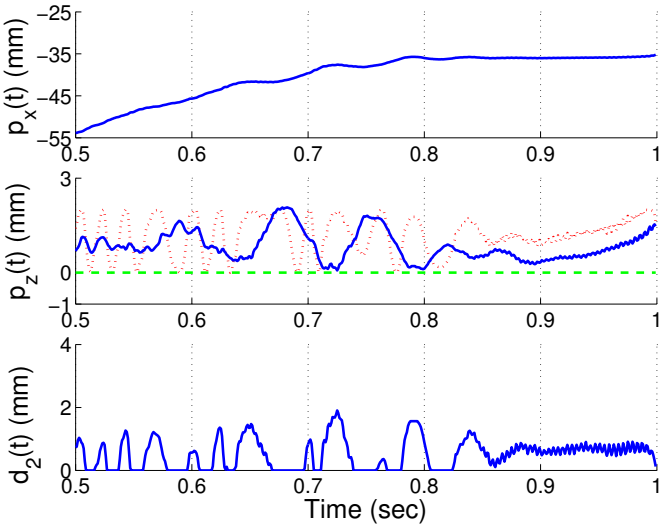

(b) Position data recorded from Exp. II-4 ($\mathbf{F}_{vec}(t)$, stroking, $d_2(t)$, and $K = 1.2$ N/mm).

Fig. 7.3. PHANToM stylus trajectories during stroking of textured surfaces rendered with different texture rendering methods. For both panels, subject S1 stroked the same textured surfaces ($A = 1$ mm and $L = 2$ mm).

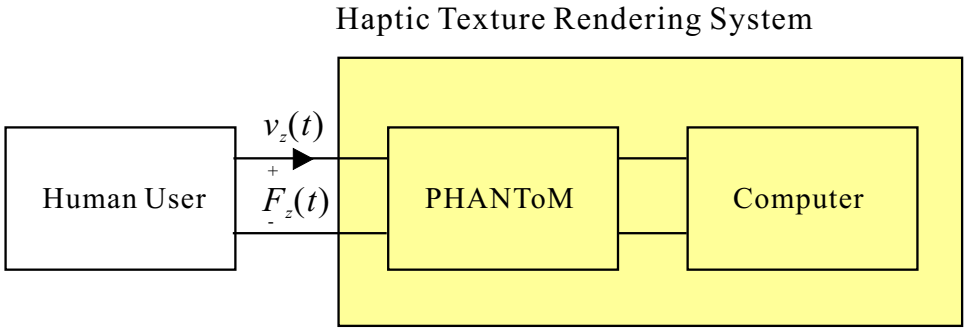

Fig. 7.4. Effort and flow of haptic texture rendering system.

7.5 Was Aliveness Caused by Device Instability?

Of the three main factors affecting the perceived stability of virtual haptic textures (environment modeling, device stability, and human perception), which factor(s) would explain the phenomenon of aliveness? To investigate this question, we examined whether it was possible for a human user to perceive aliveness while the texture rendering system including the force-feedback device was stable in the control sense. For this purpose, we applied a passivity-based stability theory on the data measured from a user interacting with virtual textured surfaces. We examined whether aliveness could be perceived from a passive (thereby stable) texture rendering system. The passivity of our texture rendering system was evaluated with a passivity observer (PO), an on-line observer for monitoring the energy flow of a dynamical system [60].

For the texture rendering system shown in Fig. 7.4, the PO with zero initial energy storage was defined as

$$PO(k) = \sum_{i=1}^{k} F_z^W(i\Delta t) v_z(i\Delta t)\Delta t, \tag{7.1}$$

where Δt was the sampling time, k was the time index for samples, $F_z^W(t)$ was the measured force at the PHANToM stylus along the z-axis of the PHANToM world coordinate frame, and $v_z(t)$ was the velocity of the stylus along the z-axis. The forces and velocities in the other directions were not considered since the $\mathbf{F}_{mag}(t)$ rendering method produced forces only in the z-direction. Due to the poor resolution of velocity estimates derived

directly from the PHANToM position encoders [75], $v_z(t)$ was estimated using an end-fit first-order adaptive windowing technique [76]. The texture rendering system was passive if the PO remained positive at all time indices under consideration [60].

Fig. 7.5 shows representative data plots for the following four cases: (a) the haptic texture rendering system was passive (hence stable) and subject reported no perceived instability during free exploration, (b) the rendering system was passive and aliveness was perceived during free exploration, (c) the rendering system was passive and aliveness was perceived during stroking, and (d) the rendering system was active and both buzzing and aliveness were perceived during stroking. In the top two subplots, the top trace was $p_z(t)$ (position in the z-direction along surface-height variation), the middle trace was $F_z^W(t)$ (force in the z-direction), and the bottom trace was PO, all recorded over 10 s. In the bottom two subplots where stroking was used, an additional trace of $p_x(t)$ (position along the direction of stroking) was added.

It can be seen from Fig. 7.5(a) that the subject was able to maintain a stationary contact between the PHANToM stylus and the virtual textured surface. Both the position and force traces exhibited no obvious abrupt changes at any time. The PO plot remained positive at all times indicating that the haptic texture rendering system was passive and stable. These data were taken with a stiffness value that was about one standard deviation below the threshold for perceptually stable texture rendering under the same condition. This was an example of a haptic texture rendering system that was stable in both perception and control.

Fig. 7.5(b) shows data measured with a stiffness value that was about one standard deviation above the threshold for stable rendering. The subject reported the perception of aliveness in this case. Consistent with the subject's perception, larger fluctuations were observed in both the $p_z(t)$ and $F_z^W(t)$ plots. However, excluding the data in the 3–5 s time interval that seemed to be the result of the subject's voluntary movement, the position change in $p_z(t)$ was relatively smaller (about 2 mm at maximum) than the force change in $F_z^W(t)$ (about 1 N at maximum) over the 10-s time period. Despite the perception of aliveness, however, the PO remained positive indicating that the texture rendering system

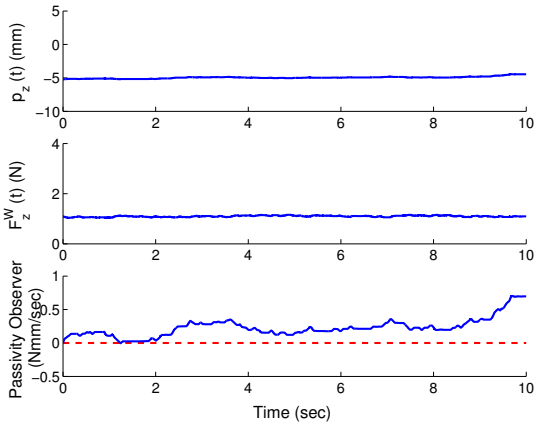

(a) A passive haptic texture rendering system without perceived instability (Subject S2, free exploration, $A = 1$ mm, $L = 2$ mm, and $K = 0.2$ N/mm).

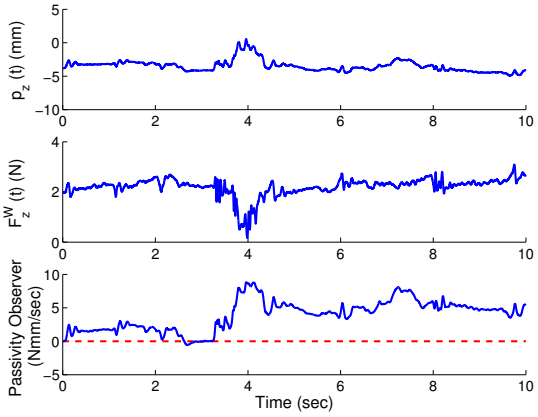

(b) A passive haptic texture rendering system with aliveness perception (Subject S1, free exploration, $A = 1$ mm, $L = 2$ mm, and $K = 0.5$ N/mm).

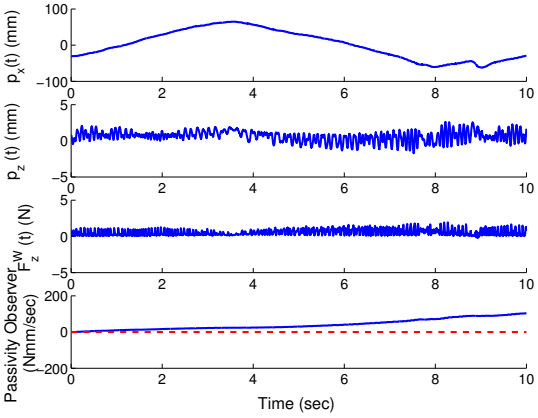

(c) A passive haptic texture rendering system with aliveness perception (Subject S1, stroking, $A = 1$ mm, $L = 2$ mm, and $K = 0.8$ N/mm).

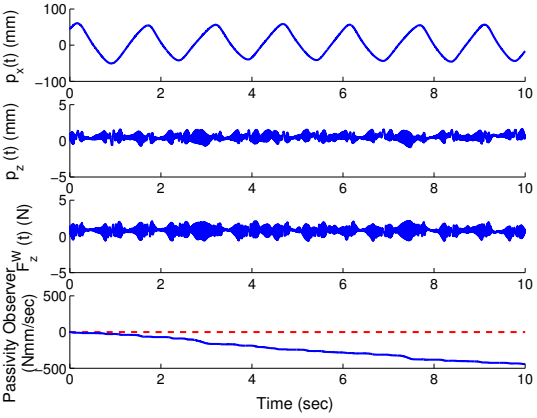

(d) An active haptic texture rendering with both types of perceived instability (Subject S2, stroking, $A = 1$ mm, $L = 2$ mm, and $K = 1.2$ N/mm).

Fig. 7.5. Representative haptic texture rendering systems with various combinations of observed passivity and perceived instability.

was passive and stable. This was an example of perceived instability despite a stable haptic texture rendering system.

A similar case was found with stroking mode. The data shown in Fig. 7.5(c) were measured with a stiffness value that was one standard deviation above the corresponding threshold for stable texture rendering. The subject reported the perception of aliveness but not buzzing. The top trace shows that the subject completed a little more than one complete stroking motion (back and forth) during the 10-s period. The next two traces ($p_z(t)$ and $F_z^W(t)$, respectively) show the abrupt changes in proximal stimuli that resulted in the perception of aliveness. In particular, the magnitude of force variations was up to about 2 N. Despite the perception of aliveness, however, the PO remained positive indicating that the texture rendering system was passive and stable. This was yet another example of perceived instability despite a stable haptic texture rendering system.

Fig. 7.5(d) shows an example where the texture rendering system was active during stroking. The data were measured when the subject stroked the textured surface rendered with a high stiffness ($K = 1.2$ N/mm). The subject reported both types of perceived instability (aliveness and high-frequency buzzing noises). Aliveness can be observed in the two traces of $p_z(t)$ and $F_z^W(t)$ in terms of very small positional variations but relatively large force variations. High-frequency buzzing was confirmed by a spectral peak at 150 Hz in the power spectrum of $p_z(t)$ that was shown earlier in Fig. 7.1(b). In the bottom trace of Fig. 7.5(d), the PO was mostly negative, indicating that the texture rendering system was active (and hence possibly unstable).

These results provide unequivocal evidence that perceived instability can occur even when a rendering system is passive and stable. We have therefore shown indirectly that environment modeling and human perception can also play important roles in perceived quality of a haptic texture rendering system. Consider the difference between touching a real and a virtual surface. When a stylus touches a real surface, it is either on or off the surface. When a stylus touches a virtual surface, however, the stylus has to penetrate the virtual surface in order for the user to form a perception of that surface through the resultant force variations. With a real surface, a stylus resting on the surface

can remain stationary due to friction (and the fact that the surface cannot be penetrated by the stylus). With a virtual surface, however, the stylus's position that can fluctuate inside the surface is amplified to perceivable forces by a texture renderer, thereby contributing to the perception of aliveness. In addition to the effect of inaccurate environment modeling, human perceptual resolution also plays an important role in the perception of aliveness. It is now well known in the literature that we tend to rely more on vision for position/movement information, and that we can easily integrate visual position information with haptic force information [77]. Our relatively poor kinesthetic resolution of unsupported hand movements in free space combined with our relatively high tactile sensitivity to force changes is also to blame for the perception of aliveness.

8. CONCLUSIONS AND FUTURE WORK

This thesis investigated the problem of *perceived instability* of virtual haptic textures with the aims to quantify conditions under which the virtual textures are perceived to be stable, to discover typical types of perceived instability, and to understand the sources of perceived instability. To achieve the three research goals, we performed psychophysical and measurement experiments in a variety of conditions differing in texture model parameter, collision detection algorithm, texture rendering method, and exploration mode using a widely-used force-feedback device called the PHANToM^{TM}. The most important conclusions to be drawn from our studies, along with the implications for realistic haptic texture rendering, are discussed below.

First, we concluded that the parameter space for perceptually stable haptic texture rendering using the PHANToM was too small to be useful in the sense that only textures that felt like soft corduroy could be rendered without any artifacts. This result significantly restricts the types of surface textures that can be properly rendered in a virtual environment or a psychophysical study. It follows that much improvement is needed in the area of haptic texture rendering in terms of perceived stability, and that many published studies might have used virtual textures that contained perceived instability.

Second, our measurements indicated that the frequency of the "buzzing" noise that contributed to perceived instability was quite intense (21.21–48.79 dB sensation level) at a relatively high frequency (192–240 Hz)[1]. In addition, measurements taken in our lab and others' revealed a mechanical resonance of the PHANToM devices at around 218 Hz. Typically, control-based studies for stable haptic interaction focus on the low-frequency dynamics of a haptic interface, since the target virtual environment (e.g., virtual flat wall) is expected to involve relatively low-frequency force commands. The perceived

[1]The values for sensation level and frequency of buzzing were taken from the results obtained with virtual haptic textures rendered with $d_1(t)$.

instability of buzzing suggests that the high-frequency dynamics can no longer be ignored in texture rendering where relatively fast and abrupt changes in force magnitude/direction can occur. It follows that the high-frequency behavior of a force-reflecting device, such as the quantization noise of encoders and flexibility of joints and links, should be considered in both theoretical and experimental studies on perceptually stable texture rendering.

Third, we were able to predict (from texture model and user stroking velocity) and then locate (from our position, force and acceleration measurements) the frequency components that conveyed texture information during stroking. This frequency range was relatively low (26–65 Hz)[2] and was well separated from that contributing to the perception of buzzing. We therefore believe that it should be possible to remove the high-frequency noise from proximal stimuli without affecting the components conveying texture information. Doing so will likely result in a significant increase of the parameter space for stable haptic texture rendering.

Fourth, our analysis suggested that the perceived instability of aliveness was caused by a relatively large change in force magnitude calculated from a relatively small change in the stylus position. Since the subject was under the impression that the stylus was held stationary in space, this force variation was attributed to an "alive" textured surface rather than the slight tremor of the subject's hand. Furthermore, we showed that the perception of aliveness could occur even when the haptic texture rendering system was passive (and therefore stable in the control sense) using a passivity-based control theory. This result provides unequivocal evidence that, unlike the case of virtual wall rendering, both the haptic texture rendering method (spring method) and the virtual texture model (sinusoidal grating) can potentially invoke the perception of unrealistic sensations such as aliveness while the haptic interface is stably controlled. To the best of our knowledge, this is the first time that anyone has demonstrated that the perceptual artifacts associated with a haptic rendering system cannot be attributed to control instabilities alone. Therefore, the development of a haptic texture rendering system needs to incorporate perceived quality

[2]This frequency range was taken from the results of the measurement experiments using $d_1(t)$.

as one of its design requirements in addition to the traditionally considered performance metrics such as computational efficiency and control stability.

Finally, the presence of "ridge instability" indicates that force directions should also be taken into account in the study of perceived instability. Texture rendering involves multidirectional interaction between the user and the rendering system. The ridge instability was mainly due to force commands that did not consider the direction of user-applied forces. As a result, the user experienced forces that seemed "active" in terms of directions. In order to render force directions that are free of direction-related perceived instability, one needs to incorporate information such as the direction of user-applied force in addition to that traditionally used in haptic rendering (e.g. position of stylus tip).

Future work to accomplish realistic rendering of virtual haptic textures will be pursued in two directions. One is to investigate the effect of other factors on perceived instability of virtual haptic textures. They include other texture models such as fractals and wavelets, and other rendering methods such as one that explicitly considers friction rendering. The other future research direction is to develop a haptic texture rendering system that guarantees realistic rendering of haptic textures. To do so requires the design of a haptic interface controller that removes control-induced instabilities such as buzzing, the development of texture rendering model and method that are free of algorithm-induced perceptual artifacts such as aliveness and ridge instability, and the evaluation of the developed systems in terms of perceived instability by human observers.

LIST OF REFERENCES

LIST OF REFERENCES

[1] S. A. Wall and W. S. Harwin, "Effects of physical bandwidth on perception of virtual gratings," in *Proceedings of the ASME Dynamic Systems and Control Division*, vol. 69, pp. 1033–1039, 2000.

[2] J. M. Weisenberger, M. J. Krier, and M. A. Rinker, "Judging the orientation of sinusoidal and square-wave virtual gratings presented via 2-DOF and 3-DOF haptic interfaces," *Haptics-e (http://www.haptics-e.org)*, vol. 1, no. 4, 2000.

[3] D. Katz, *The World of Touch*. Hillsdale, NJ: Lawrence Erlbaum Associates, 1925/1989.

[4] S. J. Lederman and M. M. Taylor, "Fingertip force, surface geometry, and the perception of roughness by active touch," *Perception & Psychophysics*, vol. 12, pp. 401–408, 1972.

[5] M. M. Taylor and S. J. Lederman, "Tactile roughness of grooved surfaces: A model and the effect of friction," *Perception & Psychophysics*, vol. 17, pp. 23–36, 1975.

[6] S. J. Lederman, J. M. Loomis, and D. A. Williams, "The role of vibration in the tactual perception of roughness," *Perception & Psychophysics*, vol. 32, pp. 109–116, 1982.

[7] S. J. Lederman, "Tactual roughness perception: Spatial and temporal determinants," *Canadian Journal of Psychology*, vol. 37, pp. 498–511, 1983.

[8] C. E. Connor, S. S. Hsiao, J. R. Phillips, and K. O. Johnson, "Tactile roughness: Neural codes that account for psychophysical magnitude estimates," *Journal of Neuroscience*, vol. 10, pp. 3823–3836, 1990.

[9] C. E. Connor and K. O. Johnson, "Neural coding of tactile texture: Comparison of spatial and temporal mechanisms for roughness perception," *Journal of Neuroscience*, vol. 12, pp. 3414–3426, 1992.

[10] R. L. Klatzky, S. J. Lederman, C. Hamilton, and G. Ramsay, "Perceiving roughness via a rigid probe: Effects of exploration speed," in *Proceedings of the ASME Dynamic Systems and Control Division*, vol. 67, pp. 27–33, ASME, 1999.

[11] S. J. Lederman, R. L. Klatzky, C. L. Hamilton, and G. I. Ramsay, "Perceiving roughness via a rigid probe: Psychophysical effects of exploration speed and mode of touch," *Haptics-e (http://www.haptics-e.org)*, vol. 1, no. 1, 1999.

[12] K. O. Johnson and S. S. Hsiao, "Neural mechanisms of tactual form and texture perception," *Annual Review of Neuroscience*, vol. 15, pp. 227–250, 1992.

[13] S. J. Lederman and R. L. Klatzky, "Feeling through a probe," in *Proceedings of the ASME Dynamic Systems and Control Division*, vol. 64, pp. 127–131, ASME, 1998.

[14] S. J. Lederman and R. L. Klatzky, "Sensing and displaying spatially distributed fingertip forces in haptic interfaces for teleoperator and virtual environment systems," *Presence*, vol. 8, pp. 86–103, 1999.

[15] M. Hollins and S. R. Risner, "Evidence for the duplex theory of tactile texture perception," *Perception & Psychophysics*, vol. 62, pp. 695–705, 2000.

[16] K. O. Johnson and S. S. Hsiao, "Evaluation of the relative roles of slowly and rapidly adapting afferent fibers in roughness perception," *Canadian Journal of Physiology & Pharmacology*, vol. 72, pp. 488–497, 1994.

[17] R. H. LaMotte and M. A. Srinivasan, "Surface microgeometry: Tactile perception and neural encoding," in *Information Processing in the Somatosensory Systems, Wenner-Gren International Symposium Series* (O. Franzen and J. Westman, eds.), pp. 49–58, MacMillan Press, 1991.

[18] R. L. Klatzky and S. J. Lederman, "Tactile roughness perception with a rigid link interposed between skin and surface," *Perception & Psychophysics*, vol. 61, pp. 591–607, 1999.

[19] M. S. O'Modhrain, "Restricted access: Exploratory procedures and object properties," in *Proceedings of the ASME Dynamic Systems and Control Division*, vol. 67, pp. 415–420, 1999.

[20] S. J. Lederman and R. L. Klatzky, "Hand movement: A window into haptic object recognition," *Cognitive Psychology*, vol. 19, pp. 342–368, 1987.

[21] S. J. Lederman and R. L. Klatzky, "Flexible exploration by human and robotic hand systems," in *Proceedings of the Annual International Conference of the IEEE Engineering in Medicine and Biology Society*, vol. 12, pp. 1915–1916, 1990.

[22] H. Iwata, H. Yano, F. Nakaizumi, and R. Kawamura, "Project FEELEX: Adding haptic surface to graphics," in *Computer Graphics (Proceedings of ACM SIGGRAPH 2001)*, 2001.

[23] Y. Ikei, K. Wakamatsu, and S. Fukuda, "Vibratory tactile display of image-based textures," *IEEE Computer Graphics and Applications*, vol. 17, no. 6, pp. 53–61, 1997.

[24] Y. Ikei, M. Yamada, and S. Fukuda, "Tactile texture presentation by vibratory pin arrays based on surface height maps," in *Proceedings of the ASME Dynamic Systems and Control Division*, vol. 67, pp. 51–58, 1999.

[25] P. S. Wellman, W. J. Peine, G. E. Favalora, and R. D. Howe, "Mechanical design and control of a high-bandwidth shape memory alloy tactile display," in *Proceedings of the 1997 International Symposium on Experimental Robotics*, 1997.

[26] T. H. Massie and J. K. Salisbury, "The phantom haptic interface: A device for probing virtual objects," in *Proceedings of the ASME Dynamic Systems and Control Division*, vol. 55–1, pp. 295–301, 1994.

[27] F. Dimension, *http://www.forcedimension.com*.

[28] P. Buttolo and B. Hannaford, "Pen based force display for percision manipulation of virtual environments," in *Proceedings of IEEE Virtual Reality Annual International Symposium*, pp. 217–225, 1995.

[29] R. L. Hollis, S. E. Salcudean, and A. P. Allen, "A six-degree-of-freedom magnetically levitated compliance fine-motion wrist: Design, modeling, and control," *IEEE Transactions on Robotics and Automation*, vol. 7, no. 3, pp. 320–332, 1991.

[30] S. E. Salcudean, N. M. Wong, and R. L. Hollis, "Design and control of a force-reflecting teleoperation system with magnetically levitated master and wrist," *IEEE Transactions on Robotics and Automation*, vol. 11, no. 6, pp. 844–858, 1995.

[31] R. J. Adams and B. Hannaford, "Stable haptic interaction with virtual environments," *IEEE Transactions on Robotics and Automation*, vol. 15, pp. 465–474, June 1999.

[32] J. M. Hollerbach and D. E. Johnson, "Virtual environment rendering." To appear in Human and Machine Haptics, 2000.

[33] R. Balaniuk and I. F. Costa, "LEM – an approach for physically based soft tissue simulation suitable for haptic interaction," in *Proceedings of the Fifth PHANToM Users Group Workship*, 2000.

[34] D. L. James and D. K. Pai, "A unified treatment of elastostatic contact simulation for real time haptics," *Haptics-e (www.haptics-e.org)*, vol. 2, no. 1, 2001.

[35] Y. Adachi, T. Kumano, and K. Ogino, "Intermediate representation for stiff virtual objects," in *Proceedings of IEEE Virtual Reality Annual International Symposium*, pp. 203–210, 1995.

[36] W. R. Mark, S. C. Randolph, M. Finch, J. M. V. Verth, and R. M. Taylor, "Adding force feedback to graphics systems: Issues and solutions," in *Proceedings of the Annual Conference on Computer Graphics (SIGGRAPH 96)*, pp. 447–452, 1996.

[37] C. B. Zilles and J. K. Salisbury, "A constraint-based god-object method for haptic display," in *Proceedings of IEEE International Conference on Intelligent Robots and Systems*, pp. 146–151, 1995.

[38] D. Ruspini, K. Kolarov, and O. Khatib, "The haptic display of complex graphical environments," in *Computer Graphics Proceedings, Annual Conference Series*, pp. 345–352, ACM SIGGRAPH 97, 1997.

[39] C. Ho, C. Basdogan, and M. A. Srinivasan, "Efficient point-based rendering techniques for haptic display of virtual objects," *Presence*, vol. 8, no. 5, pp. 477–491, 1999.

[40] K. Salisbury and C. Tarr, "Haptic rendering of surfaces defined by implicit functions," in *Proceedings of the ASME Dynamic Systems and Control Division*, vol. 61, pp. 61–67, 1997.

[41] D. E. Johnson and E. Cohen, "An improved method for haptic tracing of sculpted surfaces," in *Proceedings of the ASME Dynamic Systems and Control Division*, vol. 64, pp. 243–248, 1998.

[42] M. Minsky and S. J. Lederman, "Simulated haptic textures: Roughness," in *Proceedings of the ASME Dynamic Systems and Control Division*, vol. 58, pp. 421–426, ASME, 1996.

[43] M. D. R. Minsky, *Computational Haptics: The Sandpaper System for Synthesizing Texture for a Force-Feedback Display*. PhD thesis, MIT, June 1995.

[44] T. H. Massie, "Initial haptic explorations with the phantom: Virtual touch through point interaction," Master's thesis, MIT, Feb. 1996.

[45] J. P. Fritz and K. E. Barner, "Stochastic models for haptic texture," in *Proceedings of SPIE's International Symposium on Intelligent Systems and Advanced Manufacturing – Telemanipulator and Telepresence Technologies III*, pp. 34–44, 1996.

[46] J. Siira and D. K. Pai, "Haptic texturing - a stochastic approach," in *Proceedings of the IEEE International Conference on Robotics and Automation*, pp. 557–562, 1996.

[47] M. A. Costa and M. R. Cutkosky, "Roughness perception of haptically displayed fractal surfaces," in *Proceedings of the ASME Dynamic Systems and Control Division*, vol. 69-2, pp. 1073–1079, 2000.

[48] L. Kim, A. Kyrikou, G. S. Sukhatme, and M. Desbrun, "An implicit-based haptic rendering technique," in *Proceedings of the IEEE/RSJ International Conference on Intelligent Robots and Systems*, pp. 2943–2948, 2002.

[49] A. M. Okamura, J. T. Dennerlein, and R. D. Howe, "Vibration feedback models for virtual environments," in *Proceedings of the IEEE International Conference on Robotics and Automation*, pp. 674–679, 1998.

[50] J. E. Lloyd and D. K. Pai, "Robotics mapping for friction and roughness for reality-based modeling," in *Proceedings of the IEEE International Conference on Robotics and Automation*, pp. 1884–1890, 2001.

[51] R. B. Gillespie and M. R. Cutkosky, "Stable user-specific haptic rendering of the virtual wall," in *Proceedings of the ASME International Mechanical Engineering Congress and Exhibition*, vol. 58, pp. 397–406, ASME, 1996.

[52] A. Z. Hajian and R. D. Howe, "Identification of the mechanical impedance at the human finger tip," in *Proceedings of the ASME International Mechanical Engineering Congress, Dynamic Systems and Control Division*, vol. 55, pp. 319–327, ASME, 1994.

[53] A. J. Hodgson and N. Hogan, "A model-independent definition of attractor behavior applicable to interactive tasks," *IEEE Transactions on Systems, Man, and Cybernetics - Part C: Applications and Reviews*, vol. 30, no. 1, pp. 105–117, 2000.

[54] N. Hogan, "Multivariable mechanics of the neuromuscular system," in *Proceedings of IEEE Annual Conference of the Engineering in Medicine and Biology Society*, pp. 594–598, 1986.

[55] M. C. Çavuşoğlu, A. Sherman, and F. Tendick, "Design of bilateral teleoperation controllers for haptic exploration and telemanipulation of soft environments," *IEEE Transactions on Robotics and Automation*, vol. 18, no. 4, pp. 641–647, 2002.

[56] J. E. Colgate and G. Schenkel, "Passivity of a class of sampled-data systems: Application to haptic interfaces," in *Proceedings of the American Control Conference*, pp. 3236 – 3240, 1994.

[57] R. J. Adams, D. Klowden, and B. Hannaford, "Stable haptic interaction using the excalibur force display," in *Proceedings of the IEEE International Conference on Robotics and Automation*, 2000.

[58] B. E. Miller, E. Colgate, and R. A. Freeman, "Guaranteed stability of haptic systems with nonlinear virtual environments," *IEEE Transactions on Robotics and Automation*, vol. 16, no. 6, pp. 712–719, 2000.

[59] B. Hannaford and J.-H. Ryu, "Time domain passivity control of haptic interfaces," in *Proceedings of the IEEE International Conference on Robotics and Automation*, pp. 1863–1869, 2001.

[60] B. Hannaford and J.-H. Ryu, "Time-domain passivity control of haptic interfaces," *IEEE Transactions on Robotics and Automation*, vol. 18, no. 1, pp. 1–10, 2002.

[61] J.-H. Ryu, D.-S. Kwon, and B. Hannaford, "Stable teleoperation with time domain passivity control," in *Proceedings of the IEEE International Conference on Robotics and Automation*, pp. 3260–3265, 2002.

[62] D. Lee and P. Y. Li, "Toward robust passivity: A passive control implementation structure for mechanical teleoperators," in *Proceedings of the 11th International Symposium on Haptic Interfaces for Virtual Environment and Teleoperator Systems (IEEE VR 2003)*, pp. 132–139, 2003.

[63] B. Hannaford, J.-H. Ryu, and Y. S. Kim, "Stable control of haptics," in *Touch in Virtual Environments: Proceedings of USC Workshop on Haptic Interfaces* (M. McLaughlin, ed.), pp. 47–70, Prentice Hall, 2001.

[64] N. Hogan, "Controlling impedance at the Man/Machine interface," in *Proceedings of the IEEE International Conference on Robotics and Automation*, pp. 1626–1631, 1989.

[65] S. A. Wall and W. S. Harwin, "Modeling of surface identifying characteristics using Fourier series," in *Proceedings of the ASME Dynamic Systems and Control Division*, vol. 67, pp. 65–71, 1999.

[66] G. A. Gescheider, *Psychophysics: Method, Theory, and Application*. Lawrence Erlbaum Associates, Inc., Publishers, second ed., 1985.

[67] S. W. Smith, *The Scientist and Engineer's Guide to Digital Signal Processing*. P.O. Box 502407 San Diego, CA 92150-2407: California Technical Publishing, second ed., 1999.

[68] S. J. Bolanowski, Jr., G. A. Gesheider, R. T. Verrillo, and C. M. Checkosky, "Four channels mediate the mechanical aspects of touch," *Journal of Acoustical Society of America*, vol. 84, no. 5, pp. 1680–1694, 1988.

[69] R. T. Verrillo, "Vibrotactile thresholds measured at the finger," *Perception & Psychophysics*, vol. 9, no. 4, pp. 329–339, 1971.

[70] R. T. Verrillo, "Effect of contactor area on the vibrotactile threshold," *The Journal of the Acoustical Society of America*, vol. 35, no. 13, pp. 1962–1966, 1963.

[71] H. Z. Tan, *Information Transmission with a Multi-Finger Tactual Display*. PhD thesis, Massachusetts Institute of Technology, Cambridge, MA, 1996.

[72] V. B. Mountcastle, W. H. Talbot, I. Darian-Smith, and H. H. Kornhuber, "Neural basis of the sense of flutter-vibration," *Science*, vol. 155, pp. 597–600, 1955.

[73] R. T. Verrillo and G. A. Gescheider, "Perception via the sense of touch," in *Tactile Aids for the Hearing Impaired* (I. R. Summers, ed.), pp. 1–36, 19B Compton Terrace, London N1 2UN, England: Whurr Publishers Ltd, 1992.

[74] K. O. Johnson, T. Yoshioka, and F. Vega-Bermudez, "Tactile functions of mechanoreceptive afferents innervating the hand," *Journal of Clinical Neurophysiology*, vol. 17, no. 6, pp. 539–558, 2000.

[75] M. C. Çavuşoğlu, D. Feygin, and F. Tendick, "A critical study of the mechanical and electrical properties of the PHANToM^{TM} haptic interface and improvements for high performance control," *Presence*, vol. 11, no. 6, pp. 555–568, 2002.

[76] F. Janabi-Sharifi, V. Hayward, and C.-S. J. Chen, "Discrete-time adaptive windowing for velocity estimation," *IEEE Transactions on Control System Technology*, vol. 8, no. 6, pp. 1003–1009, 2000.

[77] M. A. Srinivasan, G. L. Beauregard, and D. L. Brock, "The impact of visual information on haptic perception of stiffness in virtual environments," in *Proceedings of the ASME Dynamic Systems and Control Division*, vol. 58, pp. 555–559, 1996.

APPENDIX

APPENDIX A
LIST OF PUBLICATIONS

This chapter of appendix provides the list of publications whose contents are based on this thesis.

A.1 Journal Articles

1. Seungmoon Choi and Hong Z. Tan, "Towards Realistic Haptic Rendering of Surface Textures," Accepted for publication in *IEEE Computer Graphics & Applications (Special Issue – Haptic Rendering Beyond Visual Computing)*, 2003.

2. Seungmoon Choi and Hong Z. Tan, "Perceived Instability of Haptic Virtual Texture. I. Experimental Studies," *Presence: Teleoperators and Virtual Environments* (in press), 2003.

A.2 Submitted Journal Articles

1. Seungmoon Choi and Hong Z. Tan, "Perceived Instability of Haptic Virtual Texture. II. Effects of Collision Detection Algorithm," Submitted to *Presence: Teleoperators and Virtual Environments*, 2003.

A.3 Peer-Reviewed Conference Papers

1. Seungmoon Choi Hong Z. Tan, "Aliveness: Perceived Instability from a Passive Haptic Texture Rendering System," In *Proceedings of IEEE/RSJ International Conference on Intelligent Robots and Systems (IROS 2003)*, pp. 2678–2683, 2003.

2. Seungmoon Choi and Hong Z. Tan, "An Experimental Study of Perceived Instability During Haptic Texture Rendering: Effects of Collision Detection Algorithm," In *Proceedings of the 11th International Symposium on Haptic Interfaces for Virtual Environment and Teleoperator Systems* (in conjunction with *IEEE VR 2003*), pp. 197–204, 2003.
3. Seungmoon Choi and Hong Z. Tan, "A Study on the Sources of Perceptual Instability During Haptic Texture Rendering," In *Proceedings of the IEEE International Conference on Robotics and Automation (ICRA 2002)*, pp. 1261–1268, 2002.
4. Seungmoon Choi and Hong Z. Tan, "An Analysis of Perceptual Instability During Haptic Texture Rendering," In *Proceedings of the 10th International Symposium on Haptic Interfaces for Virtual Environment and Teleoperator Systems* (in conjunction with *IEEE VR 2003*), pp. 129–136, 2002.

A.4 Abstract-Reviewed Conference Papers

1. Seungmoon Choi and Hong Z. Tan, "A Parameter Space for Perceptually Stable Haptic Texture Rendering," In *Proceedings of the Fifth PHANToM Users Group Workshop (PUG2000)*, J. K. Salisbury and M. A. Srinivasan (Eds.), 2000.

APPENDIX B
TECHNICAL INFORMATION FOR EXPERIMENT IMPLEMENTATION

This chapter of appendix presents the technical information regarding the equipments and programs used to implement the experiments reported in this thesis. It is our hope that the information provided in this chapter can facilitate the reuse of the equipments and programs.

B.1 Psychophysical Experiments

All directories that will be mentioned in this section for the locations of programs and data are located under File Server:\\Seungmoon\MyWork\PerceivedInstability \PsychophysicalExperiments.

B.1.1 Equipment

The experiment programs were designed for the PHANToM (model 1.0A) made by Sensable Inc. (http://www.sensable.com).

B.1.2 Programs

Two programs were used for the psychophysical experiments using $d_1(t)$ reported in Ch. 4. The first program was to generate a profile of a subject for the main experiment. This setup program was written in C/C++, and is located in \Setup\Setup_With_Discontinuity. The program asks a series of questions about the subject and experimental parameters, and

produces a text file with the extension of "cfg" that contains information necessary for the main psychophysical experiment program.

The main program for the psychophysical experiment was written in C/C++ using the GHOST software library for the PHANToM. It is located in \MainExp\ Experiment_With_Discontinuity. The program that renders a haptic virtual textured surface without any graphics, and measure stiffness thresholds for perceptually stable rendering following the rule of the method of limits. After an experiment, the program outputs a text file with the extension of "dat" that contains the results of the psychophysical experiment.

For the psychophysical experiments using $d_2(t)$ reported in Ch. 6, two similar programs were used. The programs files are stored in \Setup\Setup_Without_Discontinuity and \MainExp\Experiment_Without_Discontinuity for the setup and main experiment programs, respectively.

To reuse the main experiment programs, following actions are required. First, haptic rendering algorithm that was implemented using gstForceField class of the GHOST library for texture rendering has to be rewritten to be appropriate for one's purpose. Second, some hardcoded parameters such as the step size of stiffness increase/derease and the directories for the locations of data files have to be changed. Finally, a modified program has to be recompiled using the GHOST library whose version matches the PHANToM driver installed on a PC[1].

B.1.3 Data and analysis

The experimental results of the two psychophysical experiments are stored in \Data\Data_With_Discontinuity and \Data\Data_Without_Discontinuity, respectively. The names of data files are self-evident. Each directory has a subdirectory named as "AnalysisPrograms", which contains MATLAB scripts to plot the stiffness thresholds in various

[1]It is recommended to use the most recent version of the PHANToM driver and GHOST library (V4.0 as of December, 2003). The PHANToM driver is freely available at the manufacturer's web site, and a CD for GHOST V4.0 is available in the haptics lab library.

ways. Another subdirectory, “Figures”, contains many MATLAB figures for the results of the corresponding psychophysical experiment. Finally, the SAS scripts written for statistical data analysis are under a subdirectory of “STATAnalysis”.

B.2 Measurement Experiments

Every directory that will be mentioned in this section is referenced with respect to File Server:\\Seungmoon\MyWork\PerceivedInstability\MeasurementExperiments.

B.2.1 Equipments

The PHANToM 1.0A instrumented with two additional sensors, a 3D force/torque (F/T) sensor and a 3D accelerometer, was used to render virtual textures and measure physical variables. The F/T sensor was of model Nano 17 manufactured by ATI Industrial Automation (http://www.ati-ia.com). The F/T sensor output was connected to a temperature compensation box, and the output of the temperature compensation box was sent to the ISA-bus interface card in a PC. The detailed specification can be found in the manual of the F/T sensor that can be downloaded from the manufacturer web site.

The accelerometer was of model 8794A500 from Kistler (http://www.kistler.com). The accelerometer output was connected to a signal conditioning box (model 5134 from Kister). The signal conditioning box converted the raw acceleration readings to voltages that could be readable by a standard data acquisition card. It is also capable of amplifying the signal with an adjustable gain control and of low-pass filtering with several predefined cut-off frequencies. The data sheet of this acceleration measurement equipments is available in the haptics lab library and also downloadable from the manufacturer web site. The output of the signal conditioning box was fed to a signal connection box (model SCB 100 made by National Instruments). This signal connection box was connected to the data acquisition card (model AT-MIO-64E-3 from National Instruments) inside the PC. This model is a general-purpose data acquisition card with 64 single-ended analog input channels (12 bit resolution), 2 analog output channels (12 bit resolution) and 8 digital in-

put/output channels. The details of this model can be found in the manual (AT E Series User Manual). The manyal is also located in the haptics lab library and downloadable from the web site of National Instruments (http://www.ni.com).

To attach the F/T sensor to the PHANToM, the last link of the PHANToM needs to be replaced by the custom-made link discussed in 5.1.1. The custom-made link is composed of two pieces, and the F/T sensor can be fixed between the pieces with set screws. For a coordinate frame transformation module of the measurement experiment program to work properly, the x, y, and z axes of the F/T sensor (refer to the F/T sensor data sheet for the orientation of the F/T sensor coordinate frame) must be aligned to coincide with $-x$, $-z$, and $-y$ axes of the PHANToM world coordinate frame when the PHANToM is at the zero configuration (see Fig. 5.1 for the PHANToM world coordinate frame). The accelerometer can be installed to the PHANToM using a press-fit adapter as shown in Fig. 5.1. The local coordinate frame of the accelerometer (see the data sheet of the accelerometer) has to match the PHANToM world coordinate frame when the PHANToM is at zero configuration.

B.2.2 Programs

Two programs used to render a virtual textured surface and measure position, force, and acceleration data were made in C/C++ and are located in the directories of \MeasurementExp_DT and \MeasurementExp_CT. The program under the former directory was used for the measurement experiment using $d_1(t)$ reported in Ch. 5, and one under the latter directory was used for that using $d_2(t)$ reported in Ch. 7.

Both programs are Windows programs written using Microsoft MFC. The programs render virtual haptic textured surfaces with user specified conditions. While the textures are rendered, the programs collect raw position, force, and acceleration data, convert them appropriately, and save the results in a text file.

To control the PHANToM, the programs use the GHOST library. Again, gstForceField class was used to render virtual textures. To collect F/T sensor data, the programs

need the Active X driver for the ISA interface card of the F/T sensor to be installed on a PC. The force sensor output collection module uses the associated APIs provided by the manufacturer. Note that this module is obsolete, as the force sensor has been updated to one working with a general purpose data acquisition card after the measurement experiments. This force sensor reading module does not work any more with the current F/T sensor.[2] The data acquisition card to collect accelerometer outputs was programmed using NI-DAQ library provided by the National Instruments.

Also included in the programs is a routine that convert the force sensor reading measured in the coordinate frame of the F/T sensor to those in the coordinate frames of the PHANToM (such as the world and stylus coordinate frames). As this capability is not provided in the GHOST library in a straightforward manner, this module can be useful for who needs to do similar tasks.

To reuse the measurement experiment programs, one should do following tasks. First, one needs to write his own code for haptic rendering appropriate for his/her purpose. Second, the F/T sensor driver (available at the web site of ATI Industrial Automation) has to be installed on a PC, and the F/T sensor reading module should be modified so that it uses the data acquisition card. Finally, the NI-DAQ driver and library for the data acquisition card needs to be installed on the PC. These are freely available at the web site of National Instruments.

B.2.3 Data and analysis

The data of measurement experiments are stored in \Data\MeasurementExp_DT and \Data\MeasurementExp_CT. The data in the former directory was used to produce the results reported in Ch. 5, and those in the latter directory was for those of Ch. 7.

Each data file has an extension of "mdt". The naming convention of the data file name was made to specify the conditions under which the data file was measured. For example, the data file "MDATA_CT_SC_M_SU_A1_L1_K06.mdt" was measured from the

[2]See File Server:\\Seungmoon\MyWork\ShakerProject\Programs\DT_V3 for force sensor reading routines that work with the current F/T sensor using a data acquisition card.

sinusoidal textured surface with amplitude= 1 mm, wavelength= 2 mm, and stiffness= 0.6 N/mm. "CT" (Continuous Texture) means that the surface was rendered with the collision detection method of $d_2(t)$. For the data collected using $d_1(t)$, either "DT" (Discontinuous texture) or none was used instead of "CT". "SC" is the initial of the subject. The texture rendering method was specified at the location of "M" ("M" for $\mathbf{F}_{mag}(t)$ and "B" for $\mathbf{F}_{vec}(t)$). Finally, "SU" means that it was for Stroking exploration mode ("F" for free exploration) and for an Unstable case ("S" for a stable case).

Each of the data directories has two additional subdirectories, "AnalysisPrograms" and "Figures". As the name suggests, the "AnalysisPrograms" has various MATLAB scripts used to analyze the measured data in the time and frequency domains. Some of the MATLAB scripts include a module to generate a flat-top window that is not directly supported in MATLAB. The "Figures" directory has MATLAB figures for the analysis results.

B.3 PHANToM Tip Inertia Measurement

Programs and data for the measurement of the apparent tip inertia of a PHANToM are under File Server:\\Seungmoon\MyWork\PerceivedInstability \PHANToMCharacterization\PHANToMTipInertiaMeasurement.

B.3.1 Equipment

The tip inertia of any model of PHANToM can be measured with the program that will be introduced in the next subsection.

B.3.2 Program

The program can be found in \Program directory. Based on user specified conditions (for example, axis for inertia measurement), this program actuate the PHANToM and record the positions of the PHANToM stylus tip. The results are saved in a text file.

B.3.3 Data and analysis

The data measured using the original PHANToM 1.0A and the instrumented PHANToM are stored in the subdirectories of \Data\DefaultPHANToM and \Data \InstrumendPHANToM, respectively. To process the data, the MATLAB script "PlotData.m" can be used. This script generates data plots and compute the apparent tip inertia based on the measured data.

B.4 PHANToM Frequency Response Measurement

Programs and data for the measurement of the frequency response of a PHANToM are under File Server:\\Seungmoon\MyWork\PerceivedInstability \PHANToMCharacterization\FrequencyResponse.

B.4.1 Equipment

The frequency response of any type of PHANToM can be measured with the following program.

B.4.2 Program

The program is located in \Program subdirectory. This program measures the frequency response of the PHANToM at the origin of the PHANToM coordinate frame for the frequency range of 1–500 Hz. For each frequency, the program drives the PHANToM with a force command of a sine waveform at the frequency, and measures the resulting position of the stylus tip. The measured data are recorded in a text file for further analysis.

B.4.3 Data and analysis

The data measured using the PHANToM 1.0A can be found in \Data subdirectory. There are 500 data files with names "sineXXX.dat", where XXX means the frequency

with which that the data file was measured. MATLAB scripts such as “FR_Sine_flattop.m” in the same directory can be used to extract the magnitude of the frequency response at the frequency from the power spectrum density of the measured position data. The final results are summarized in “Frequency_Response_Origin.m”.

B.5 Passivity Observer

Programs used to judge the passivity of a haptic texture rendering system can be found under File Server:\\Seungmoon\MyWork\PerceivedInstability \PHANToMCharacterization\PassivityObserver.

B.5.1 Programs

The MATLAB scripts in which the passivity observer was implemented are in \Programs directory. “PassivityObserver.m” is the main script. In “Vel_end_fit_FOAW.m” and “Vel_best_fit_FOAW.m”, the velocity estimation techniques in [76] are implemented as MATLAB functioins. These two files are called from “PassivityObserver.m” file.

B.5.2 Data and analysis

To run the programs for passivity analysis, one need a data file that has position and force records. In the thesis, the data collected in the measurement experiments were used for passivity analysis of the texture rendering system. The results of the analysis are summarized in the various plots under \Figures directory.

VITA

VITA

Seungmoon Choi was born in Busan, Republic of Korea on 1971. After graduating from BaeMyung High School in Seoul, Korea, he entered the Department of Control and Instrumentation Engineering at Seoul National University, Korea in 1991 and received a B.S. degree in 1995. He began his graduate study in the same department under the supervision of Prof. BeomHee Lee in 1995, and received a M.S. degree in 1997 for his work on robot control and motion planning. Since 1998, he has been conducting his Ph.D. research in the School of Electrical and Computer Engineering at Purdue University under Prof. Hong Z. Tan. His research in haptics focuses on the rendering and perception of virtual haptic textures.